“Neotectonics” in the northern African margin: new paleomagnetic constraints from northwestern Algeria

Mohamed El-Messaoud Derder, Saïd Maouche, Philippe Robion, Bernard Henry, Mohamed Amenna, Souhila Hassina Boukerbout, Yves Missenard, Boualem Bayou, Rafik Bestandji, Aziouz Ouabadi

"Neotectonics" in the northern African margin: New paleomagnetic constraints from northwestern Algeria

Mohamed El-Messaoud Derder[1], Saïd Maouche[1], Philippe Robion[2], Bernard Henry[3], Mohamed Amenna[1], Souhila Hassina Boukerbout[1], Yves Missenard[4], Boualem Bayou[1], Rafik Bestandji[1] and Aziouz Ouabadi[5].

[1] CRAAG, BP 63, 16340 Bouzaréah, Alger, Algeria

[2] CY Cergy Paris Université, Geosciences Environment Cergy, 5 mail Gay-Lussac, 95031 Cergy-Pontoise cedex France

[3] Université de Paris, Paléomagnétisme, Institut de Physique du Globe de Paris, Sorbonne Paris Cité and UMR 7154 CNRS, 1 rue Jussieu, 75238 cedex 05, France.

[4] GEOPS, CNRS UMR8148, Univ. Paris-Sud, Université Paris-Saclay, Rue du Belvédère, Bât. 504, 91405 Orsay, France.

[5] Laboratoire "Géodynamique, Géologie de l'Ingénieur et Planétologie", FSTGAT / USTHB, BP 32, El-Alia Bab Ezzouar, 16111 Alger, Algeria

Corresponding author: Derder M.E.M. *Tel: +213 23 18 90 98; Fax: +213 23 18 91 01* m.e.m.derder@gmail.com. Orcid ID: 0000-0003-0212-7294

Abstract.

Previous paleomagnetic studies performed in the central North-Algeria (Chellif and Mitidja basins) on Neogene formations pointed out tectonic clockwise blocks rotations. This deformation pattern was interpreted as resulting from a bookshelf neotectonics, consequence of the Africa-Eurasia plates convergence. A new paleomagnetic study was conducted on the Neogene volcanic rocks outcropping in the Northwestern Algeria (Marset Ben Mhidi - Aïn Temouchent – Tifaraouine area). The obtained stable remanent magnetization is mainly carried by Ti-poor titanomagnetite. The paleomagnetic data show that, since the lava emplacement, the northwestern Algeria underwent a mean moderate clockwise block-rotations of 9.3° ± 4.5°. For the Algerian margin, this confirms a context of transpression and blocks rotations in a strike-slip tectonic setting. A decreasing deformation gradient from the E to the W affected the different basins of this margin, from strong rotations within the Mitidja, to the moderate ones in the Chellif and to Marset Ben Mhidi - Aïn Temouchent – Tifaraouine area where rotations magnitudes are significantly lower.

Keywords: Northwestern Algeria, Paleomagnetism, Structural corrections, Aeromagnetic data, Neotectonics, Block rotation, Transpression.

Introduction

The seismic activity of the Western Mediterranean area is mainly concentrated in northern Africa, especially in northern Algeria (see Meghraoui 2018 and references herein). That was highlighted for example by the significant earthquakes of El Asnam 10 October 1980 Ms= 7.3 (Ouyed et al. 1981) and Zemmouri 21 May 2003 Mw=6.9 (Ayadi et al. 2003). This earthquake activity is associated with the active tectonics in relation with the convergence between Africa and Eurasia plates (Le Pichon et al. 1988; Dewey et al, 1989; Ricou 1994). A counterclockwise rotation of Africa with respect to Eurasia since Upper Cretaceous has been established from magnetic anomaly studies in the Atlantic Ocean (Dewey et al. 1989; Mazzoli and Helman 1994; Rosenbaum et al. 2002 and references therein), inducing this convergence. Geodetic models using GPS data (Nocquet and Calais 2004; Serpelloni et al. 2007) also support this convergence as well as the associated transpression tectonic system for the recent times (Meghraoui and Pondrelli 2012). Such convergence involves transpression tectonics, with N-S to NNW-SSE shortening direction, giving active deformation along the plate boundary (Morel and Meghraoui 1996; Mauffret 2007).

The north-western Algeria belongs to an active continental margin, a fold-and-thrust belt located on the southern side of the western Mediterranean considered as the plate boundary between Africa and Eurasia. In this region, the focal mechanisms of recent earthquakes and related stress distribution display consistent WNW-ESE to E-W right-lateral strike slip faults and NE-SW trending reverse faults (Meghraoui 1991; Meghraoui et al. 1996; Maouche et al. 2011, 2019; Ousadou et al. 2014; Benbakhti et al. 2018; Abouda et al. 2019). The northern Algeria margin appears to be structured by these regional major E-W to WNW-ESE dextral shear zones (Thomas 1976). Between them, the main active structures, affecting intermountain and coastal Neogene to Quaternary sedimentary basins (e.g., Cheliff and Mitidja), are NE-SW trending folds and NE-SW sinistral transpressive faults delimiting NE-SW oriented blocks (Thomas 1985: Mauffret et al. 1987; Meghraoui et al. 1996). The active deformation has been modeled as dominated by bookshelf blocks rotation (Ron et al. 1984; Nur et al. 1986; see Hernandez-Moreno et al. 2014) in northern Algeria (Meghraoui and Pondrelli 2012). The transpressive tectonics system with NNW-SSE direction of convergence then should imply clockwise rotations of these blocks. The aim of the present work is to look after the prior activity of this system in the same convergence frame.

In the central part of northern Algeria (Cheliff and Mitidja basins), paleomagnetic studies were already performed on Neogene sedimentary and magmatic formations (Aïfa et al. 1992; Derder et al. 2011; 2013; 2019). Part of the obtained paleomagnetic directions correspond to sites affected by local rotations along faults. The other ones (given here after tilt correction) indicate clockwise rotations (Fig. 9), for the Cheliff (11-7 Ma, prefolding data: N = 9, D = 31.1°, I = 56.0°, k = 33, α_{95} = 9.1° - Derder et al. 2011) and Mitidja (16-11Ma; N = 17, D = 232.3°, I = -16.5°, k = 37, α_{95} = 5.9° - Derder et al. 2019) basins. They evidenced tectonic clockwise rotation of large blocks, in some cases even of large magnitude, as expected in the kinematic model (Meghraoui and Pondrelli 2012). Narrow zones, corresponding to important shear zones including smaller blocks, are affected by strong rotations (Derder et al. 2013, 2019). In a large area (about 100 km wide in longitude as in latitude) located west of the Cheliff basin, around Aïn Temouchent and Ghazaouet cities, Neogene volcanic rocks are largely present. Bellon and Guardia (1980), using paleomagnetic investigations in a limited zone, evidenced normal and reversed magnetizations close to the direction of the recent magnetic field. Results analysis was however not performed using the present reliable standards, introducing significant uncertainty on these data. A new study was then carried out on a much larger scale in different areas where calco--alkaline and alkaline volcanic rocks, from Miocene to Quaternary in age, outcrop (Fig. 1a). Complementary field structural and aeromagnetic data analyses were performed to help for paleomagnetic results interpretation. The use of aeromagnetic data in this study was also important since it allows identifying "magnetized" structures in depth, (both onshore and offshore), which favored the present, (but also past), deformations with rotations in the northern Algeria margin.

Geological setting

The northwestern Algeria area belongs to the external domain of the Tell Atlas belt (Guardia 1975). It extends parallel to the Mediterranean coast from the Algerian-Moroccan border to the Dahra range (Northern side of the Cheliff basin) and is characterized by nappes covered by Neogene to Quaternary sediments and volcanic rocks. The Upper Miocene and Pliocene deposits postdate the nappes emplacement (Guardia, 1975; Thomas, 1985). The Quaternary sedimentation is mainly represented by marine and alluvial terraces. This area is also characterized by an intense volcanic activity dated between 14.97 and 0.82 Ma (Bellon and Guardia 1980; Bellon et al. 1984; Louni-Hacini et al. 1995; Coulon et al 2002). This inland volcanism is represented by three main facies, initially (Upper Miocene) rhyolitic and andesitic and in a second period (Pleistocene) basaltic, (Megartsi 1985; Guardia 1975). Considering the

nature and the given age of the volcanic series, Coulon et al. (2002) subdivided this sector into 6 distinct zones (Fig. 1a). The basaltic emissions are particularly important in the Ain Temouchent area (zone 2) while volcanism in the Tafna area (zones 3 and 4) is of andesitic nature. The coastal sector in the zone 1 is marked by rhyodacitic type while dacitic rocks constitute the Habibas Island, located 13 km offshore. Tuffs and breccias are visible in this island and along the continental coast (zone 1). The figure 1a shows the volcanic rocks areas distribution in relation with their nature and age.

Structures such as reverse faults with asymmetrical folds, normal and strike slip faults and nappes, constitute the main tectonic features in this part of Tell Atlas. Concerning the "post-nappes" tectonics, several observations have been made:

- Along the coastal northern zone 1, still active folding process is attested by the deformation of Quaternary marine terraces. In this area, juxtaposed and tilted marine terraces, mainly related to vertical motion, can be observed on the northern side of the Murdjadjo anticline (Benbakhti et al. 2018; Fig. 1a).
- The Benzekri NE-SW fault-related fold (Fig. 1a), activated during the Temouchent 22 December 1999 Mw = 5.7 earthquake (Belabbes et al. 2009), is one of the major fold structure, similar to that (Murdjadjo, Tamazoura) observed in the Habra basin borders, (Benbakhti et al. 2018; Meghraoui 1988; Bouhadad et al. 2001).
- NNE-SSW faults can be observed in all the studied area.
- N-S normal faults, observed along the Tafna River, evidenced a pull-apart system for a Tafna basin (Sadran 1958; Guardia 1975).
- Except very locally, the rocks were only affected by brittle deformations.

The flows mostly show weak to moderate dip (Tab. 1), rather suggesting emplacement on slopes. However, the location of the Neogene volcanic activity in northwestern Algeria seems to be juxtaposed to the main faults affecting this region (Sadran 1958; Guardia 1975; Thomas 1976, 1985; Louni-Hacini 2002). In the Ain Temouchent area (Fig. 1a), the volcanic centers are almost aligned along a NNE-SSW direction, confirming the relationship between volcanism and tectonics (Sadran 1958; Guardia 1975; Thomas 1976, 1985). Sadran (1958) and Megartsi (1985) highlighted this tectonic direction also in the Middle (along the Traras border fault) and Lower Tafna areas (Fig. 1a), both affected by the volcanic activity.

Methodology, sampling, and analytical procedure.

The magnetic data used for the aeromagnetic analyses derived from the airborne survey, flown over Algeria between 1969 and 1974, by Aero Service Corporation (constant flight

altitude of 150 m and along N20W lines 2 km spaced out, with perpendicular tie-lines at 5 km intervals). The measurement along profiles was about every 46 m. As the aeromagnetic data were on map (scale of 1/200000) of total field intensity, the data covering the studied area were digitized and 9801 points were obtained. The digitized values of the total magnetic field intensity were interpolated to a spacing grid of 230m x 230m. The magnetic anomaly map (Fig. 2a) was then obtained by subtracting the normal field established for the aeromagnetic survey period (Boukerbout and Abtout, 2010) using the Algerian repetitive network data.

Paleomagnetic analyses have been already successfully used in such structural context (e.g., Henry, 1992; Hernandez-Moreno et al. 2014). Here we focused on volcanic large bodies, of different ages, cropping out in 6 main areas (Coulon et al. 2002) around Marset Ben Mhidi - Aïn Temouchent – Tifaraouine (Fig. 1a). They were extensively sampled for the paleomagnetic investigations: 831 cores distributed over 79 sites (Fig. 1b). Sedimentary rocks were also studied in 7 sites (58 cores). All cores were oriented with magnetic and sun compasses.

One to three specimens of standard size have been cut from each core, allowing pilot specimens demagnetization and additional rock magnetic studies. Before any demagnetization analysis, the specimens were stored in zero magnetic field for at least one month to reduce a possible viscous magnetization. The remanent magnetization was measured using JR5 spinner magnetometer (AGICO, Brno, Czech Republic) in the CRAAG Algiers laboratory. Both thermal (TH) and Alternating Field (AF) demagnetizations were performed on pilot specimens, using for AF a Molspin AF Demagnetizer; TH demagnetization was made using a cylindrical furnace (ASC Model TD48-SC) with a fast heating-rate (45 minutes to reach 680°C) while forced air enhanced the cooling (20 minutes). In order to appropriately separate and recognize the magnetization components, numerous demagnetization steps were used. Used increments range from 50-100°C for the lowest temperatures to 10°C for the highest ones for the TH, and from 1 mT to 10 mT for the AF (maximum used field intensity: 100 mT). The results of demagnetization process were presented on orthogonal vector plots (As and Zijderveld, 1958; Zijderveld 1967). The remaining magnetization vectors after each step and the difference vectors removed between two consecutive demagnetization steps were plotted on equal area projections. The direction of the magnetization components was calculated by principal component analysis (Kirschvink 1980). Mean paleomagnetic directions were determined using Fisher's statistics (Fisher 1953) and presented on equal area projections.

Rock-magnetic measurements were performed in the GEC laboratory (CY Cergy-Paris University). K(T) thermomagnetic curves (low-field magnetic susceptibility K as a function of

temperature T) have been measured on AGICO KLY3, CS3 equipment. Hysteresis loops were obtained from Micro-Mag VSM equipment.

Results

Aeromagnetic data.

The obtained map (Fig. 2) shows important anomalies, and that the most "magnetized" zones are located along the coast and up to 40 km offshore. They correspond to high susceptibility rocks, such as magma intrusions during volcanic events. From magnetic standpoint, this means that the structures responsible of these anomalies are deeply rooted, affecting the crust.

To identify the magnetic anomalies causative structures, the wavelet and ridgelet transforms processing were used (Boukerbout and Gibert, 2006; Boukerbout et al. 2018a; 2018b). These methods lead to a 3-D image (Fig. 2b) showing thus the main deep structures in the studied area, covered by aeromagnetic data. Most of them are in depth and range between 2 and 8 km, other ones being at greater depths. These anomalies correspond to the part of the structures affected by magmatic intrusions, and these structures could reach higher depths. Most of them are NNE-SSW to NE-SW trending. E-W and NW-SE to WNW-ESE trends correspond to structures 3 and 2, respectively.

Most identified deep structures roughly correlate with surface faults (Fig. 1a), such as the NNE-SSW and E-W ones. Offshore, new structures are identified showing the continuity of the structural frame. Relatively to Figure 1a, the results, obtained from aeromagnetic data processing, add key information on the vertical and lateral extension of the main structures with their connection at depth.

Rockmagnetism

The Natural Remanent Magnetization (NRM) has a rather high intensity, varying from 1.1 10^{-5} A/m to 92.9 A/m, with a mean of 3.3 A/m. Most variations of the intensity during thermal demagnetization show, after effects related to a viscous magnetization, a progressive decrease of the magnetization intensity up to around 550-580°C (Fig. 3a - MG655 and BS14 samples), indicating Ti-poor titanomagnetite as magnetic carrier. For other samples, a change in the slope of the demagnetization curve occurs at about 300-400°C (Fig. 3a - MG599 and BS505 samples), suggesting the presence of maghemite. For the samples of the site 49 (zone 4) and for all samples of the zone 6, the magnetization decreases up to 580°C followed by a change in the slope of the demagnetization curve for temperatures higher than 580 °C (Fig. 3a - MB888 and MB882 samples), pointing out the presence of both Ti-poor titanomagnetite and hematite.

Typical samples from different sites of volcanic rocks were selected for complementary experiments to better specify their magnetic mineralogy and characteristic properties.

K(T) curves for most sites, as exemplified on figure 3b, show an increase of magnetic susceptibility up to ~ 300°C. Partial cooling loops carried out from this temperature shows that no significant mineralogical alteration occurred. For temperature higher than 300°C, a progressive decrease of susceptibility is observed, giving Curie point at about 550-580°C, arguing for Ti-poor titanomagnetite as main magnetic carrier. These samples show practically reversible magnetization during the heating-cooling process, except a slight alteration that occurred at the highest temperatures, giving separation in two components visible only on the cooling curve below 400°C.

In sites belonging to the zone 6 (Fig. 3d), the first decrease between 300 and 450°C is followed by a second decrease from 500 up to 580°C. The variation shown by the first decrease does not appear on the cooling curve, contrary to that corresponding to the second one. That suggests a first decrease related to transformation of maghemite in hematite and a second one to primary Ti-poor titanomagnetite. A third small decrease for temperature higher than 580°C indicates the presence of hematite, possibly resulting of the inversion of the maghemite.

In few other samples, the magnetic mineralogy appears to be even a little bit different. The figure 3c shows a peak on heating and cooling curves around 100°C, evidence of the presence of a stable component, likely Ti-rich titanomagnetite. During heating, a first mineralogical transformation starts at around 300-400°C, pleading in favor of the presence of maghemite that transforms in hematite (visible by a weak remaining susceptibility for temperatures higher than 580°C). A very weak decrease up to 580°C could be due to Ti-poor titanomagnetite. During the higher temperature treatment, a second transformation occurs, resulting in new minerals, mainly magnetite, visible on the cooling curve below 580°C.

Hysteresis loops from most samples (Fig. 3e) show low mean coercive force and remanent coercive force, about 6 and 17 mT, respectively and complete magnetization saturation at about 0.4 to 0.5 T. This argues in favor a low coercivity component (like Ti-poor titanomagnetite). However, few loops corresponding to samples having maximum unblocking temperature higher than 580 °C, show a wasp-waisted shape (Fig. 3f). They also have higher partial saturation, around 1 T, and do not reach total saturation (signifying the presence of an additional high coercivity component). The mean coercive force and remanent coercive force are in these cases somewhat higher (30 and 43 mT, respectively), confirming a mixing of low and high coercivity components (e.g., Ti-poor titanomagnetite and hematite).

In conclusion, Ti-poor titanomagnetite is the main magnetic carrier in these volcanic rocks, but, in few sites, Ti-rich titanomagnetite, maghemite and hematite were also present.

Paleomagnetic results

After selection from pilot specimen analysis, 661 samples have been demagnetized. Obtained paleomagnetic direction is similar using either TH, AF or combined AF-TH demagnetizations processes (Fig. 4). In some sites, in particular all the sedimentary ones, remanent magnetization intensity is too weak to be analyzed. For this reason, 7 weathered volcanic sites and all non-volcanic sites were discarded. In the other sites, two different main cases were observed from Zijderveld diagrams.

- The first one, obtained on most samples, yields a single stable magnetic B component, obtained after elimination of a secondary viscous A magnetization. In the site 38, obtained stable directions are too scattered (lightning effect?) to give reliable mean direction and results from this site will be not further considered. During AF demagnetization, the intensity decrease is regular up to elimination of almost all the remanent magnetization (Figs. 4b and c), except in the zone 6 where about 40% of this magnetization remains (Fig. 4d). This remaining magnetization can be deleted in this case only by TH treatment for temperatures up to at least 650°C (Fig. 4e). That clearly highlights the presence of both magnetite and hematite in these samples. In this case, no difference appears between paleomagnetic directions carried by magnetite and hematite (Fig. 4d and e), indicating formation of the hematite during or very few after lava emplacement (for example in relation with high temperature fumaroles – e.g., Stoiber and Rose, 1974). The obtained Characteristic Remanent Magnetization (ChRM) B is of normal or reversed polarity according to the sites.
- The second type is related to other samples displaying erratic evolution during demagnetization process, not allowing reliable paleomagnetic results.

The mean B ChRM directions from 67 mean site data (reversed directions recalculated as normal polarity data) is defined by D = 9.3°, I = 49.8°, k = 33, α_{95} = 3.1 ° and D = 10.8 °, I = 45.8 °, k = 22, α_{95} = 3.8°, before and after bedding correction, respectively. These two directions are not significantly different. Detailed data are presented in the figure 5 and tables 1 and 2.

Structural corrections

The bedding correction for volcanic rocks could be disputable, since a "slope" may already have existed at the emplacement time. For example, a "slope" on the flanks of a rhyodacitic dome can be related to lava emplacement. In volcanic areas, lava flows often emplaced on a preexisting slope, generally but not always moderate (e.g.,Henry et al. 2003). In

such areas, the slope direction depends on local topographic conditions, related for example to the shape of the volcanic edifice or to previous flows. It is rarely coherent at a regional scale, except if the slope is related to a coherent folding prior to the volcanism. Sub-horizontal emplacements are mainly limited to particular cataclysmic cases (e.g., volcanic traps). An opposite case is represented by pyroclastic flows that can mold an existing complicated topography (e.g., Alva-Valdivia et al. 2005). In some cases, the volcanic eruptions were associated to a local uplift due to magma ascent (for example in rift zones – e.g., Hildenbrand et al. 2012), giving, around the uplifted area, slope that will guide the flow emplacement. Later, this slope can be often increased, due to the continuation of the uplift (Silva et al. 2018). That can be evidenced with a progressive "untilting", i.e., the analysis of the dispersion of the paleomagnetic directions (given by the k precision parameter of Fisher 1953) as a function of the untilting percentage. The untilting percentage associated with the best solution (minimum dispersion) corresponds to the actual "dip" during magnetization acquisition, i.e., to the slope during the volcanic flow emplacement (Silva et al. 2018). In the northwestern Algeria, two different cases can be distinguished.

- Except in part of the zone 1 (Fig. 1a), "dip" directions measured on the field are very scattered, without any clear dominant orientation. The figure 6 shows the orientation of the associated strikes. Such scattering indicates that these "dips" are not related to a regional folding with a uniform orientation of all the fold axes. All "dip" values are moderate (mean value 15°; only 3 values higher than 30°, with a maximum of 45°). Scattering of "dip" directions and moderate "dip" values suggest lavas emplaced on local slopes. In addition, Bellon and Guardia (1980) indicated that, within the eastern part of the zone 6 (Fig. 1a), flow direction had variable orientation. The progressive untilting (Fig. 7) gives optimal tilting correction in average about 20% untilting (between 0 and 35% - Table 1), indicating a moderate slope increase (corresponding to only around 20% of the total "dip") after lavas emplacement. In the different zones, retained tilting correction (corresponding to the optimal untilting percentage) is assumed to restore the slope during the volcanic rocks emplacement. The post-emplacement "dip" variation should be related to local uplift due to magma ascent or fault movement. It could actually give a tilting toward a direction different from that of the initial slope. That is why a small circle approach (e.g., Surmont et al. 1990; Henry et al. 2004b, Calvin et al. 2017) cannot be used here. Owing to the moderate "dip" values, that introduces only a weak uncertainty on the calculated corrected direction. Such uncertainty does not concern the zones 4-5 where optimal untilting is around 0%, indicating the absence of significant tilting after lavas emplacement.

- In the coastal part of the zone 1, a dominant "dip" direction toward SE to SSE clearly appears (Fig. 6), suggesting that this zone was affected by a more or less homogeneous tilting.

The structural corrections "at optimal untilting" can be considered as the best approximate solution. Owing to the moderate "dip" values and the scattering of the dip directions, the obtained statistical mean direction (D = 9.3°, I= 49.1°, k =35, α_{95} =3.0°) appears to be not significantly different from that at 0% and 100% untilting (Fig. 5, Tab. 2). The choice of the applied structural corrections will have therefore no actual effect for the interpretation in terms of regional rotation.

Reversal test (McFadden and McElhinny 1990)

Reversal tests (Fig. 5, Tab 3) are positive in all zones whether in geographic or stratigraphic coordinates, with the only exception of the zones 4-5 that give a negative test in stratigraphic coordinates (confirming the best untilting at 0% in these zones). In all zones, the angular difference (γ) between the mean normal and the mean reversed directions has the lowest value for the optimal untilting (Tab. 3), corroborating the reliability of this bedding correction. Using the whole data set, this test is negative in geographic coordinates, in stratigraphic coordinates and for the optimal untilting. This is due to the data from zone 1 that present a different paleomagnetic direction (Tab. 2).

Although the assumption of a remagnetization cannot be definitively ruled out in case of positive reversal test (Henry et al. 2004a), this confirms that magnetization is highly likely primary.

Discussion

Major structures

Field observations and aeromagnetic data highlight mainly NNE-SSW to NE-SW and E-W faults. Analyses of the aeromagnetic data demonstrate that at least part of them are not limited to a "surface" tectonics and on the contrary are major deep-seated structures affecting the crust.

Paleomagnetic data

The A_{95} value, obtained for the paleomagnetic pole associated with our 55 ChRMs from the zones 2 to 6 with neighboring paleomagnetic directions (λ = 78.6°N, Φ = 105.8°E, K = 30, A_{95} = 3.5°), is within the envelope (between A_{95Min} and A_{95Max}) defined by Deenen et al. (2011, 2014) as corresponding to a distribution associated with the paleosecular variation: A_{95} = 3.5° for A_{95Min} = 2.4° and A_{95Max} = 6.6°. That is also verified for the different zones (Tab. 2). The

presence of directions reflecting the paleosecular variation clearly indicates the primary character of the magnetization. That again strongly argues for the reliability of the obtained results.

The expected mean paleomagnetic directions in the studied area, for the age of the volcanism and according to the Apparent Polar Wander Path (Besse and Courtillot 2002), are between -0.3° and 0.8° for the declination and 49.1° and 51.2° for the inclination. The obtained mean inclination in our sites matches perfectly with these values, whereas the obtained declination suggests that the studied area underwent a mean clockwise rotation of the order of 9.3° ±4.5° (Desmarest 1983).

The comparison of the paleomagnetic data by age (Tab. 2) seems not to be reliable for two reasons. First, the age for most zones is actually based only on few sites (see Coulon et al. 2002) and generalization to all sites within some zones, particularly in the southernmost ones, is doubtful. Second, for the oldest age (only found in zones 1, 4 and 6 - Coulon et al. 2002), the structural evolution seems have been different in zone 1 and in the southern zones, including the zones 4 and 6 (Fig. 8, see above).

A global comparison by magnetic polarity should have been meaningless, because considered period includes several reversals.

Local deformation

The obtained paleomagnetic directions for each zone can however be compared with each other (Tab. 2 and Fig. 8). They are not statistically different. Only declination present differences for zones 1 and 2 relatively to the other zones. In both cases, number of studied sites is significant, but that is insufficient to constrain a global block rotation geometry (Hernandez-Moreno et al. 2014).

- The declination in zone 1 suggests a weak counterclockwise rotation relatively to the expected directions, and a rotation difference of the order of 15° relatively to the zones 3 to 6.
- In zone 2, difference in declination is much lower, of the order of 6° relatively to the values obtained in zones 3 to 6. No abrupt variation appears relatively to the neighboring zone 3 and no coherent variation within this zone 2. That suggests a very weak bending in this zone close to the Benzekri fault-related fold.

The measured "dip" values are moderate and mainly due to an "initial" slope. An interesting implication of the analyses of the structural corrections could concerns a local chronology of the "magmatic period". 65 to 100% of this moderate "dip" was acquired before the volcanic eruptions, i.e., corresponding to weak slopes. These "movements" could be partly related to this volcanism by prior activity of the faults that will be the future magma feeder and

inflation due to the magma ascent (e.g., Silva et al. 2012, 2018). These initial slopes could also simply correspond to topography of previous flows. However, in part of the zone 1, a relatively coherent dip direction suggests an effect of folding with NE-SW axis (Fig. 6) before the lava emplacement (about 90% of the dip acquired before magnetization acquisition). Such fold axis orientation corresponds to that of the neighboring Murdjadjo fold (Fig. 8) limiting the Habra basin to the northwest. This last fold is similar to the Benzekri fault-related fold (Fig. 1a) and to those observed in the Chellif and Mitidja basins.

Regional deformation

The obtained paleomagnetic data indicates moderate rotations of the different studied zones. The figure 8 highlights the key tectonic structures, which could provide a corresponding interpretative frame (see (Hernandez-Moreno et al. 2014): The NNE-SSW structures should be sinistral strike-slip-faults (Thomas 1974), separating blocks that rotated within a bookshelf system. The dextral WNW-ESE to E-W faults, visible to the north and to the south of the studied area, could be the major structures bounding this system (Fig. 9). The northern area (zone 1) which is not affected by the same rotations, is in a particular structural position between neighboring WNW-ESE dextral strike-slip faults, likely explaining this evolution by a smaller size and a more equidimensional shape of the block (Fig. 8).

At the Tell Atlas scale, a bookshelf system has been evidenced in the different basins. It allows the regional shortening of the Maghrebian northern border related to the NNW-SSE Europe-Africa convergence. The NNW-SSE shortening is also partly absorbed in the studied area by the Murdjadjo and Benzekri NE-SW fault-related folds, as in the Chellif and Mitidja basins by similar structures (Meghraoui 1991; Meghraoui and Doumaz 1996; Maouche et al. 2011; Abouda et al. 2019).

Conclusions

The first stage of the deformation resulting from the regional Neogene NNW-SSE shortening was therefore fault related folds system growth and thrusting structures, giving a restricted shortening. In a second stage, a more important shortening would be started in relation with a large strike-slip context, resulting in blocks rotations within simple bookshelf systems and local moderate deformations. This structural frame shows that all the northern Algeria is a narrow E-W active zone, structured in tectonic blocks affected by rotations. These rotations are clockwise and not homogeneous in north Algeria (Fig. 9). A decreasing rotation gradient is evidenced from the Mitidja basin affected by strong rotations (in average 56°) to Marset Ben Mhidi - Aïn Temouchent – Tifaraouine area, located westward, where magnitude of the mean

rotation is limited to about 9°. For the Chellif active basin located between these two areas, the highlighted average rotation is of the order of 30°. Toward East, in the western Sicily Maghrebian belt, huge clockwise rotations up to 140° have been evidenced (Speranza et al. 2018 and references herein). All these obtained results using paleomagnetic tool are key data regarding geodynamic evolution of the Western Mediterranea with regard to the Africa-Europe plate boundary during the Neogene and Quaternary period. An open question is then the reliability of this model of block rotation tectonics for other regions along the northern Africa boundary. That underlines the importance of future works particularly in eastern Algeria, Morocco and Tunisia.

Acknowledgments

This project is supported by the collaboration between the Centre de Recherche en Astronomie Astrophysique et Géophysique (CRAAG - Algeria) and the CY Cergy Paris Université (France). We are grateful to Fabio Speranza, an anonymous reviewer and the associate editor for useful constructive comments.

References

Abouda M, Maouche S, Bouhahad Y, Belhai D (2019) Neotectonics and active tectonics of the Dahra- Lower Cheliff Basin (Tell Atlas, Algeria): Seismotectonic implication. J Afr Earth Sci 153, 250-267.

Alva-Valdivia L.M, Rosas-Elguera J, Bravo-Medina T, Caballero C, Rivas M L, Urrutia-Fucugauchi J, Goguitchaichvili A, Henry B (2005) Paleomagnetic and AMS studies of the San Gaspar ignimbrite (Trans-Mexican Volcanic belt): implications for tectonics and emplacement conditions. J Volcanol Geotherm Res 147, 68-80.

Aïfa T, Feinberg H, Derder M E M, Merabet N (1992) Rotations paléomagnétiques récentes dans le bassin du Chéliff (Algérie). Compt rend Acad Sci Paris 314, II, 915-922

As J A J Zijderveld J D A (1958), Magnetic cleaning of rocks in paleomagnetic research. Geophys. J Roy astron Soc 1, 308-319.

Ayadi A, Maouche S, Harbi A, Meghraoui M, Beldjoudi H, Oussadou F, Mahsas D, Benouar D, Heddar A, Rouchiche Y, Kherroubi A, Frogneux M, Lammali K, Benhamouda F, Sebaï A, Bourouis S, Alasset P.J, Aoudia A, Cakir Z, Merahi M, Nouar O, Yelles K, Bellik A, Briole P, Charade O, Thouvenot F, Semane F, Ferkoul, Deramchi A, Haned S A (2003) Strong Algerian earthquake strikes near capital city. EOS Trans, Amer Geophys Union 84, 561

Belabbès S, Meghraoui M, Çakir Z, Bouhadad Y (2009) InSAR analysis of a blind thrust rupture and related active folding: The 1999 Ain Temouchent earthquake (M w 5.7, Algeria) case study. J Seismology 13 (4): 421–432, doi:10.1007/s10950-008-9135-x

Bellon H, Guardia P (1980) Le volcanisme alcalin plio-quaternaire d'Algérie occidentale. Etude radiométrique et paléomagnétique. Revue de Géographie Physique et de Géologie Dynamique 22, 213-220.

Bellon H, Guardia P Magne J (1984) Les associations volcaniques du Miocène supérieur de la région Oranaise. Géologie Méditerranéenne 11, 255-264.

Benbakhti I, Maouche S, Belhai D, Harbi A, Ritz J.-F, Rabai G, Rezouk A Doumaz F (2018) Characterizing the active tectonics in the Oran region (Algeria) and recasting the 1790 earthquake. J Seismol 22,1549–1561 doi:10.1007/s10950-018-9784-3.

Besse J, Courtillot V (2002). Apparent and true polar wander and the geometry of the geomagnetic field over the last 200 Myr. J Geophys Res 107, 2300, doi:10.1029/2000JB000050.

Bouhadad Y (2001) The Murdjajo, Western Algeria, fault related fold: implications for seismic hazard. J Seismol 5:541–558. doi:10.1023/A:1012039900248

Boukerbout H and Gibert, D (2006) Identification of sources of potential fields with the continuous wavelet transform: Two-dimensional ridgelet analysis. Journal of Geophysical Research, Vol. 111, B07104, doi: 10.1029/2005JB004078.

Boukerbout H, Abtout, A (2010) Le champ aéromagnétique algérien: champ magnétique total ou champ d'anomalie? Bull. Serv. Géol. Natl. vol. 21 (2), 183–200.

Boukerbout H, Abtout A and Bouyahiaoui B (2018a) Identification of magnetic lineaments from aeromagnetic data in the Northwest of Algeria. 7ème Colloque Maghrébin de Géophysique Appliquée. CMGA7, Février 2018, Algiers.

Boukerbout H, Abtout A, Gibert D, Henry B, Bouyahiaoui B and Derder M E M (2018b). Identification of deep magnetized structures in the tectonically active Chlef area (Algeria) from aeromagnetic data using wavelet and ridgelet transforms. Journal of Applied Geophysics, 154, 167-181.

Calvin P, Villalaín J J, Casas-Sainz A M, Tauxe L, Torres-Lopez S (2017) pySCu: A new python code for analyzing remagnetizations directions by means of small circle utilities. Comput Geosc 109, 32–42

Coulon C, Megartsi M, Fourcade S, Maury R.C, Bellon H, Louni-Hacini A, Cotten J, Coutelle A, Hermitte D (2002) Post-collisional transition from calc-alkaline to alkaline

volcanism during the Neogene in Oranie (Algeria): magmatic expression of a slab breakoff. Lithos 62, 87– 110

Deenen M H, Langereis C G, van Hinsbergen D J, Biggin A J (2011) Geomagnetic secular variation and the statistics of palaeomagnetic directions. Geophys J Int, 186: 509-520

Deenen M H, Langereis C G, van Hinsbergen D J, Biggin A J (2014) Erratum: Geomagnetic secular variation and the statistics of palaeomagnetic directions. Geophys J Int 197: 643, doi: 10.1093/gji/ggu021

Demarest, H.H. (1983), Error analysis for the determination of tectonic rotation from paleomagnetic data. J. Geophys. Res.88, 4321-4328.

Derder M E M Henry B, Amenna M, Bayou M, Maouche S, Besse J, Abtout A, Boukerbout H, Bessedik M, Bourouis S Ayache M (2011) Tectonic Evolution of the Active "Chelif" Basin (Northern Algeria) from Paleomagnetic and Magnetic Fabric Investigations. In New Frontiers in Tectonic Research at the Midst of Plate Convergence Intech Publisher book, 3-26, Intech Publisher, ISBN 978-953-307-594-5

Derder M E M Henry B, Maouche S, Amenna M, Bayou B, Besse J, Bessedik M, Belhai D Ayache M (2013) Transpressive tectonics along a major E-W crustal structure on the Algerian continental margin: block rotation revealed by paleomagnetic investigations. Tectonophysics. 593: 183-192.

Derder M E M, Djellit H, Maouche M, Henry B, Amenna M, Bestandji R, Ymel H, Gharbi S, Abtout A Dorbath C (2019) Strong neotectonic block-rotations, related to the Africa-Eurasia convergence, in northern Algeria: paleomagnetic evidence from the Mitidja basin. In “Geodynamics, Crustal and Lithospheric Tectonics, and active deformation in the Mediterranean Regions (A tribute to Prof. Renato Funiciello”) M. Meghraoui, L. Jolivet, R.s Wortel, S. Conticelli Eds. Tectonics 38, 4249-4266. https://doi.org/10.1029/2018TC005394.

Dewey J F, Helman M L, Turco E, Hutton D H W, Knott S.D (1989) Kinematics of the western Mediterranean. In: M.P. Coward, D. Dietrich and R.G. Park (Editors), Alpine tectonics. Geol Soc, London, 265-283.

Fisher R (1953) Dispersion on a sphere. Proc. R. Soc. London, Ser. A, 217: 295-305.

Guardia P (1975) Géodynamique de la marge alpine du continent africain d'après l'étude de l'Oranie nord-occidentale. Thesis, Nice, 289p.

Henry B (1992) Structural implications of paleomagnetic data from Pelvoux-Belledonne area (French Alps). Tectonophysics, 216: 327-338

Henry B, Camps P, Plenier. G (2003) Post-emplacement tilting of lava flows inferred from magnetic fabric study: the example of Oligocene lavas in the Jeanne d'Arc peninsula (Kerguelen islands). J Volcanol Geotherm Res127: 153-164

Henry B, Merabet N, Derder M E M, Bayou B (2004a) Chemical remagnetizations in the Illizi basin (Saharan craton, Algeria) and their acquisition process, Geophys J Int 156, 200-212

Henry B, Rouvier H, Le Goff M (2004b) Using syntectonic remagnetizations for fold geometry and vertical axis rotation: the example of the Cévennes border (France). Geophys J Int 157, 1061–1070. http://dx.doi.org/10.1111/j.1365-

Hernandez-Moreno C, Speranza F, Di Chiara A (2014), Understanding kinematics of intra-arc transcurrent deformation: Paleomagnetic evidence from the Liquiñe-Ofqui fault zone (Chile, 38–41°S), Tectonics, 33, 1964–1988, doi:10.1002/ 2014TC003622.

Hildenbrand A, Marques F O, Costa A C G, Sibrant A L R, Silva P F, Henry B, Miranda J M, Madureira P (2012) Reconstructing the architectural evolution of volcanic islands from combined K/Ar, morphologic, tectonic, and magnetic data: the Faial Island example (Azores). J Volcanol Geotherm Res 241–242, 39-48. Doi: 10.1111/j.1365-246X.2011.05320.x

Kirschvink J L (1980) The least-squares line and plane and the analysis of palaeomagnetic data. Geophys J Roy astron Soc 62, 699–718.

Le Pichon X, Bergerat F, Roulet M J (1988) Plate kinematics and tectonic leading to Alpine belt formation: a new analysis, Processes in continental lithospheric deformation. Geol Soc Amer Spec Paper 111-131.

Louni-Hacini A, Bellon H, Maury R C, Megartsi M, Coulon C, Semroud B, Cotten J, Coutelle A (1995) Datation 40K–40Ar de la transition du volcanisme calco-alcalin en Oranie au Miocène supérieur. C. R. Acad. Sci. Paris, série IIa 321, 975–982.

Louni-Hacini A (2002) La transition du magmatisme calco-alcalin au magmatisme alcalin dans l'Oranie (Algérie nord occidentale), PhD Thesis, Algiers University, 201p.

Maouche S, Meghraoui M, Morhange C, Belabbes S, Bouhadad Y, Hadoum H (2011) Active coastal thrusting and folding, and uplift rate of the Sahel Anticline and Zemmouri earthquake area (Tell Atlas, Algeria). Tectonophysics, 509, 69-80. Doi:10.1016/j.tecto.2011.06.003.

Maouche S, Bouhadad Y, Harbi A, Rouchiche Y, Ousadou F, Ayadi A (2019) Active Tectonics and Seismic Hazard in the Tell Atlas (Northern Algeria): A Review. The Geology of the Arab World — An Overview, Springer Geology, 381-400.

Mauffret A, (2007) The Northwestern (Maghreb) boundary of the Nubia (Africa) plate. Tectonophysics 429, 21–44.

Mauffret A, El Robrini M, Gennesseaux M (1987) Indice de la compression récente en mer Méditerranée : un bassin losangique sur la marge algérienne. Bull Soc géol France (8), III, 6, 1195-1206.

Mazzoli S, Helman M (1994) Neogene patterns of relative plate motion for Africa– Europe: some implications for recent central Mediterranean tectonics. Geol Rund 83, 464– 468

McFadden P L, McElhinny M W (1990) Classification of the reversal test in palaeomagnetism. Geophys J Int 103, 725-729.

Megartsi M (1985) Le volcanisme mio-plio-quaternaire de l'Oranie nord-occidentale. PhD Thesis, Algiers University, 270p.

Meghraoui M (1988) Géologie des zones sismiques du Nord de l'Algérie : paléosismologie, tectonique active et synthèse sismotectonique. PhD Thesis, Paris 11 University.

Meghraoui M (1991) Blind reverse faulting system associated with the Mont Chenoua-Tipasa earthquake of 29 October 1989 (north-central Algeria). Terra Nova 3, 84–93

Meghraoui M, F Doumaz (1996) Earthquake-induced flooding and paleoseismicity of the El Asnam (Algeria) fault-related fold. J Geophys Res 101, 17617–17644.

Meghraoui M (2018). Earthquake Faulting and Their Implications for the Seismic Hazard Assessment Along the Plate Boundary in North Africa. *In* A. Kallel et al. (eds.), Recent Advances in Environmental Science from the Euro-Mediterranean and Surrounding Regions, Advances in Science, Technology and Innovation. doi.org/10.1007/978-3-319-70548-4_15.

Meghraoui M, Morel J L, Andrieux J, Dahmani M (1996) Tectonique plio-quaternaire de la chaîne tello-rifaine et de la mer d'Alboran. Une zone complexe de convergence continent-continent. Bull Soc géol France, 167, 1, 141-157.

Meghraoui M, Pondrelli S (2012) Active faulting and transpression tectonics along the plate boundary in North Africa. Ann.Geophys 55, 5, 2012; doi: 10.4401/ag-4970

Morel J L, Meghraoui M (1996) Goringe-Alboran-Tell tectonic zone; a transpression system along the Africa-Eurasia plate boundary Geology 24, 8, 755-758.

Nocquet J M, Calais E (2004) Geodetic measurements of crustal deformation in the western Mediterranean and Europe. Pure Appl Geophys 161, 661–681 doi10.1007/s00024-003-2468-z

Nur A, Ron H, Scotti O (1986) Fault mechanics and the kinematics of block rotation. Geology, 14, 746-749

Ousadou F, Dorbath L, Ayadi A, Dorbath C, Gharbi, S (2014) Stress field variations along the Maghreb region derived from inversion of major seismic crisis fault plane solutions. Tectonophysics 632, 261–280

Ouyed M, Meghraoui M, Cisternas A, Deschamp A, Dorel J, Frechet F, Gaulon R, Hatzfeld D, Philip H (1981) Seismotectonics of the El Asnam earthquake. Nature 292, 5818, 26-31

Ricou L E (1994) Tethys reconstructed: Plates continental fragments and their boundaries since 260 Ma from Central America to South-eastern Asia. Geodin Acta 7, (4), 169-218.

Ron H, Freund R, Garfunkel Z. Nur A (1984) Block rotation by strike slip faulting: Structural and paleomagnetic evidence. J. Geophys. Research, 89, B7, 6256-6270.,

Rosenbaum G, Lister G S, Duboz C (2002) Relative motions of Africa, Iberia and Europe during Alpine orogeny. Tectonophysics 359, (1-2), 117-129

Sadran G (1958) Les formations volcaniques tertiaires et quaternaires du Tell Oranais. Publications du Service de la Carte Géologique de l'Algérie (Nouvelle Série), 18, 534p.

Serpelloni E, Vannucci G, Pondrelli S, Argnani A, Casula G, Anzidei M, Baldi P, Gasperini P (2007) Kinematics of the Western Africa-Eurasia plate boundary from focal mechanisms and GPS data. Geophys J Int 169, 1180–1200.

Silva P F, Henry B, Marques F O, Hildenbrand A, Madureira P, Mériaux C, Kratinova Z (2012) Palaeomagnetic study on lavas of a sub-aerial volcanic ridge (São Jorge Island, Azores) for the past 1.3 Myr: evidences for the Cobb Mountain Subchron, volcano flank instability and tectono-magmatic implications. Geophys J Int 188, 959-978.

Silva P F, Henry B, Marques F O, Hildenbrand A Lopes A, Madureira P, Madeira J, Nunes J C, Roxerova Z (2018) Volcano-tectonic framework of a linear volcanic ridge (Faial-Pico ridge, Azores Archipelago) assessed by paleomagnetic studies. J Volcanol Geotherm Res 352, 78-91.

Speranza F, Hernandez- Moreno C, Avellone G, Morticelli M G, Agate M, Sulli A, Di Stefano E (2018) Understanding Paleomagnetic Rotations in Sicily: Thrust Versus Strike- Slip. Tectonics 37, 1138-1158. https://doi.org/10.1002/2017TC004815

Stoiber R E, Rose W I (1974) Fumarole incrustations at active central American volcanoes. Geochimica et Cosmochimica Acta, 38, 495-516.

Surmont J, Sandulescu M, Bordea S (1990). Mise en évidence d'une réaimantation fini- crétacée des séries mésozoïques de l'unité de Bihor (Monts Apuseni, Roumanie) et de sa rotation horaire ultérieure. Compt rend Acad Sci Paris 310, 213–219.

Thomas G (1974) La phase de compression pléistocène en Algérie nord-occidentale: âge, premiers éléments cinématiques, relation avec les mouvements en distension, Compt rend Acad Sci Paris Série D, 279, 311–314.

Thomas G (1976) Mise en évidence de décrochements dextres est– ouest d'âge Quaternaire en Algérie nord-occidentale, Compt rend Acad Sci Paris Série D, 283, 893–896.

Thomas G (1985) Géodynamique d'un bassin intramontagneux: le bassin du bas Chéliff occidental (Algérie) durant le Mio-Plio-Quaternaire, PhD Thesis, Pau University, France.

Yelles-Chaouche A K, Djellit H, Beldjoudi H, Bezzeghoud M, Buforn E (2004) The Ain Temouchent (Algeria) Earthquake of December 22nd, 1999. Pure appl geophys 161, 607–621

Zijderveld J D A (1967) AC demagnetization of rocks: analysis of results. In: D.W. Collinson, K. M. Creer, S.K. Runcorn, (Eds.), Method in Paleomagnetism. Elsevier, Amsterdam, 254–,286.

Figures caption

Fig. 1 – (a): Geological map (after Coulon et al. 2002, modified) of the studied area (Thomas, 1976, 1985; Belabbès et al. 2009; Benbakhti et al. 2018) divided on 6 volcanic zones (Coulon et al. 2002) : 1: Miocene and post-Miocene sediments; 2: Volcanic rocks; 3: Pre-Miocene sediments; 4: Sampling sites; 5: Different volcanic zones; 6 : Faults, 7 : Thrust faults ; 8 : Folds, 9: Nappes front. Available ages in Ma for the volcanic rocks (Coulon et al, 2002) are 11.7 to 9 (Zone 1), 1.28 to 0.82 (Zone 2), 2.7 to 1.4 (Zone 3), 9.2 to 7.1 and 3.9 to 3.3 (Zone 4), 2.1 (Zone 5) and 10 and 7.5 (Zone 6). (b): Map with the sampling paleomagnetic sites distributed in the 6 different zones.

"**Fig. 2 –** (a) Magnetic anomalies map, (b) emplacement of the magnetized deep structures identified from magnetic anomalies in the studied area (inland and sea up to 40 km from the seashore) R and Gh correspond to Rachgoun and Ghazaouet cities.

Fig. 3 – Rockmagnetism: Variation of the magnetization intensity during thermal treatment in representative samples (a). Typical thermomagnetic curves K(T) for samples BS45 (b), BS21 (c) and MB895 (d). Typical hysteresis loops after correction for paramagnetism, for samples MG670 (e) and MG 623 (f). Hcr is the remanent coercive force, Field H in Tesla

Fig. 4 - Orthogonal vector plots (filled circles: horizontal plane, crosses: vertical plane), in stratigraphic coordinates for samples BS50 (a), BS63 (b), BS77 (c) and MB880 (d).

(Alternating Field demagnetization – AF (b, c), (Thermal demagnetization - TH (a) and combined AF-TH analysis (d), with insert (e) of demagnetization curves for samples of the same site. For comparison, BS50 (TH) and BS63 (AF) were sampled in a same site.

Fig. 5 - Equal-area plot showing the paleomagnetic directions (crosses and open dots in the lower and upper hemispheres, respectively) obtained from the different mean-sites B ChRM and associated mean normal and reversed directions (stars) with their confidence zone in red.

Fig. 6 - Rose diagram of the strike directions (data in percentages) in zone 1 compared to all other zones.

Fig. 7. - Normalized value k/k_{Max} of the precision parameter k (Fisher, 1953) of the B ChRM distribution during progressive untilting in the different zones. Data with same dip for neighboring sites were merged as a single datum.

Fig. 8 – Mean paleomagnetic direction (green arrows), with the associated α_{95} uncertainty (in white), in the 6 studied zones (see Fig. 1) and expected direction for stable Africa (circled black arrow).

Fig. 9 – Global blocks rotations and structural model of the North Central and Northwestern Algeria; 1: Strike slip, 2: Thrust faulting, 3: Folds, 4: Rotation; inset indicates locations of the Tafna, Cheliff and Mitidja basins, Arrows indicate the obtained paleomagnetic direction and the Expected paleomagnetic Direction (ED). Faults are from Thomas 1985; Meghraoui 1988, 1991; Belabbès et al. 2009; Maouche et al. 2011; Benbakhti et al. 2018.

Table 1 - Paleomagnetic data obtained from different sites and different zones (grey color for sedimentary sites). λ and $\phi$are the latitude and longitude of the sites; n_{mes} and $n_{ret,}$ the number of measured and retained samples, respectively. M is the mean magnetic moment of the site. P and G are the dip and the azimuth of the down-dip direction (in degrees). D_g, I_g, D_s, I_s D_o, I_o are the declination and the inclination at geographic, stratigraphic coordinates and at optimal untilting, respectively (in degrees). α_{95} (in degrees) and k are the Fisher parameters.

Table 2 - Paleomagnetic data obtained for the different zones and for different volcanism ages:. N is the number of sites; see also caption of Table 1. A_{95} is associated with paleomagnetic poles from VGPs. A_{95Min} and A_{95Max} were calculated according to Deenen et al. (2011, 2014).

Table 3 - Reversal test (McFadden and McElhinny, 1990) in the different zones. Angular difference between mean normal and mean reversed directions (γ) with its critical value (γ_c).

	Sites	λ (°N)	φ (°W)	n_{mes}	n_{ret}	M (A/m)	P(°)	G(°)	D_g(°)	I_g(°)	D_o(°)	I_o(°)	D_s(°)	I_s(°)	α_{95}(°)	k
ZONE 1 Optimal untilting 11%	34	35°38'21.1''	1°03'45.8''	8	8	0.25	20	110	352.0	52.4	354.4	53.3	20.2	57.4	7.6	148
	35	35°37'56.2''	1°04'19.0''	8	8	0.52	17	140	344.4	3.9	344.5	5.5	345.9	19.3	7.3	58
	36	35°37'56.2''	1°04'19.0''	7	7	0.28	17	140	330.1	24.3	330.2	26.0	332.2	41.0	4.7	166
	37	35°37'56.3''	1°04'18.9''	10	10	0.15	14	140	348.4	57.1	349.5	58.3	4.8	68.5	10.6	53
	38	35°36'12.6''	1°07'03.4''	8	0	3.44	38	30	-	-	-	-	-	-	-	-
	39	35°34'34.2''	1°10'08.3''	7	7	0.89	13	150	7.5	49.4	8.5	50.4	19.9	58.8	3.1	383
	40	35°34'34.2''	1°10'08.3''	7	7	0.71	13	150	15.1	30.9	15.7	31.8	22.0	39.5	4.8	257
	41	35°34'18.6''	1°10'11.0''	7	7	0.0007	13	150	340.8	36.1	341.0	37.4	343.3	48.8	9.4	52
	42	35°36'19.4''	1°06'36.0''	8	8	0.42	45	15	355.7	42.5	356.9	38.2	0.9	-0.8	10.2	44
	43	35°35'14.8''	1°07'48.1''	8	8	0.08	9	180	345.2	46.5	344.9	47.4	342.1	55.1	11.0	31
	44	35°35'11.3''	1°07'56.0''	6	6	1.31	9	180	4.2	31.2	4.2	32.1	4.7	40.2	6.8	128
	76	35°43'19.8''	1°08'05.5''	11	3	0.10	25	65	0.5	55.4	3.7	54.2	23.0	40.0	14.0	79
	77	35°43'20.2''	1°08'04.1''	11	7	0.36	25	65	353.6	51.8	356.6	50.9	16.1	38.9	4.1	218
	78	35°43'16.0''	1°07'59.9''	9	0	0.0003	25	65	-	-	-	-	-	-	-	-
	79	35°43'13.1''	1°07'58.5''	5	3	0.0004	25	65	315.8	51.8	318.9	52.6	349.2	52.9	22.6	31
	80	35°43'16.6''	1°07'57.4''	9	8	0.0006	25	655	1.0	51.5	3.7	50.3	20.9	36.4	7.4	57
ZONE 2 Optimal untilting 20%	1	35°15'47.7''	1°09'17.3''	10	10	5.39	15	230	9.2	48.0	6.6	50.5	354.3	58.1	3.3	222
	2	35°15'39.8''	1°08'28.7''	10	10	5.03	15	340	230.2	-53.5	226.1	-52.2	214.3	-46.4	6.1	65
	3	35°16'49.0''	1°14'32.4''	10	0	0.003	13	317	-	-			-	-	-	-
	4	35°16'37.4''	1°08'0.04''	10	9	1.30	10	357	194.6	-52.2	193.8	-50.1	191.6	-42.6	4.2	155
	5	35°16'15.0''	1°08'09.9''	10	10	2.04	18	350	222.2	-58.1	217.5	-55.5	206.7	-45.7	5.9	68
	6	35°18'01.2''	1°09'36.0''	10	7	4.76	9	30	212.0	-56.6	211.9	-54.6	211.7	-47.6	5.1	140
	7	35°18'10.3''	1°10'21.6''	10	7	6.03	14	38	1.5	48.4	3.5	45.8	8.5	36.6	3.9	37
	8	35°18'36.6''	1°20'09.7''	10	9	0.005	14	55	184.8	-56.8	188.3	-54.7	197.2	-46.6	7.1	53
	17	35°15'00.0''	1°11'07.2''	10	10	2.36	6	355	197.7	-32.3	197.4	-31.1	196.2	-27.8	6.2	61
	18	35°12'52.6''	1°11'35.1''	9	7	0.95	8	245	191.6	-29.8	190.7	-30.9	187.5	-34.3	6.6	85
	19	35°11'51.5''	1°11'17.0''	8	6	2.37	6	290	211.1	-46.6	209.7	-46.8	204.7	-47.4	7.1	90
	20	35°12'16.6''	1°09'42.6''	7	7	1.49	6	260	169.5	-42.2	168.3	-42.2	164.1	-41.9	7.9	60
	21	35°11'39.8''	1°10'10.6''	8	7	1.14	8	270	167.6	-50.1	165.5	-49.7	158.8	-47.8	4.5	177

	22	35°13’15.7’’	1°12’58.8’’	16	8	14.87	10	300	166.7	-51.8	164.7	-50.2	159.1	-44.4	7.9	50
	23	35°18’05.2’’	1°10’15.0’’	8	7	8.13	12	90	8.3	57.0	12.4	56.5	25.0	53.5	5.5	121
	24	35°15’46.9’’	1°15’13.2’’	8	8	1.96	6	35	151.2	-59.0	153.2	-58.4	159.4	-56.0	6.4	76
	25	35°16’44.5’’	1°16’33.8’’	8	8	2.86	6	340	210.5	-55.0	200	-54.1	204.6	-50.9	5.7	95
	26	35°16’37.5’’	1°13’12.4’’	3	0	0.0005	0	0	-	_	-	-	-	-	-	-
	27	35°16’46.5’’	1°13’08.8’’	8	5	2.28	0	0	198.9	-38.9	198.9	-38.9	198.9	-38.9	3.5	471
	28	35°17’05.0’’	1°17’56.3’’	5	0	0.0046	13	355	-	-	-	-	-	-	-	-
	29	35°18’19.9’’	1°16’17.5’’	8	6	2.89	8	250	198.5	-52.6	196.6	-53.7	189.0	-57.1	4.9	186
	30	35°15’00.0’’	1°11’07.2’’	5	0	0.0002	0	0	-	-	-	-	-	-	-	-
	31	35°18’01.7’’	1°16’11.8’’	8	6	3.61	8	250	201.0	-47.2	199.5	-48.4	193.5	-52.1	6.3	113
	32	35°18’59.0’’	1°17’13.7’’	9	7	1.92	20	120	228.6	-59.9	235.6	-58.2	253.2	-49.3	5.4	125
	33	35°18’59.0’’	1°17’13.7’’	16	6	3.34	30	123	209.4	-47.4	216.7	-47.4	239.1	-41.2	7.4	82
	T5	35°16’38.6’’	1°08’05.4’’	15	11	2.21	15	45	201.3	-59.0	203.3	-55.9	208.0	-44.9	4.0	132
	T6	35°16’38.6’’	1°08’05.4’’	10	4	2.66	28	340	46.7	54.1	39.3	51.2	22.7	37.3	7.4	154
	T10	35°15’30.0’’	1°15’13.0’’	11	8	2.46	15	285	199.2	-45.9	195.7	-46.1	187.6	-38.0	6.3	79
ZONE 3 Optimal untilting 35%	9	35°18’26.5’’	1°22’51.8’’	8	0	0.0007	12	45	-	-	-	-	-	-	-	-
	10	35°17’53.0’’	1°26’45.7’’	9	5	2.73	15	280	2.9	51.1	356.6	50.2	346.1	47.0	7.0	122
	11	35°18’07.4’’	1°28’02.6’’	9	7	2.06	20	50	353.3	51.6	359.9	47.4	8.6	38.3	6.0	101
	12	35°14’35.9’’	1°30’18.4’’	9	3	5.78	25	110	199.8	-47.0	209.1	-46.3	224.3	-41.6	14.7	71
	13	35°14’35.9’’	1°30’18.4’’	10	0	38.29	23	360	-	-	-	-	-	-	-	-
	14	35°14’48.1’’	1°29’30.8’’	10	8	3.09	20	25	17.8	61.3	19.1	54.4	20.4	41.4	4.4	156
	15	35°15’03.2’’	1°27’09.0’’	10	6	1.48	10	210	192.1	-48.8	190.7	-52.1	187.4	-58.2	6.3	113
	16	35°15’03.2’’	1°27’09.0’’	10	9	5.39	10	210	177.9	-39.5	176.3	-42.4	172.4	-47.7	4.6	124
	T7	35°17’37.3’’	1°25’24.8’’	8	3	1.56	10	330	209.5	-51.5	205.9	-49.6	200.2	-45.7	11.6	114
	T8	35°17’48.8’’	1°27’28.8’’	12	6	1.59	20	60	344.9	56.7	354.5	54.3	8.3	47.5	4.6	213
	T9	35°16’13.0’’	1°30’09.1’’	9	0	3.17	20	305	-	-	-	-	-	-	-	-
ZONE 4 Optimal untilting	45	34°56’21.8’’	1°40’16.0’’	10	5	7.69	17	40	22.4	52.2	22.4	52.2	26.8	35.8	12.0	41
	46	34°56’21.1’’	1°41’02.1’’	8	6	2.57	11	160	198.1	-34.2	198.1	-34.2	203.8	-42.5	5.8	133
	47	34°57’04.4’’	1°42’15.7’’	7	7	6.94	23	30	9.0	40.9	9.0	40.9	13.0	19.0	4.7	169
	48	34°58’03.2’’	1°42’31.9’’	8	8	4.92	10	55	348.6	29.6	348.6	29.6	353.2	25.2	3.4	272

0%	49	34°56’14.7’’	1°42’34.1’’	6	6	2.12	10	140	206.8	-31.9	206.8	-31.9	213.1	-35.4	3.7	324
	50	34°54’41.3’’	1°43’27.3’’	6	6	3.88	16	259	359.1	44.9	359.1	44.9	342.8	45.4	3.7	324
	51	34°57’39.2’’	1°45’47.6’’	10	9	2.95	30	330	5.0	40.6	5.0	40.6	356.8	14.6	6.6	62
	59	34°57’04.9’’	1°35’35.7’’	10	8	7.18	15	356	12.0	55.4	12.0	55.4	7.9	40.8	6.4	77
	60	34°57’06.1’’	1°35’26.7’’	0	0	-	15	356	-	-	-	-	-	-	-	-
	61	34°57’48.9’’	1°39’11.3’’	13	13	5.57	10	210	10.8	51.5	10.8	51.5	5.2	60.8	4.4	88
	62	34°54’52.5’’	1°48’30.2’’	0	0	-	28	15	-	-	-	-	-	-	-	-
	63	35°03’27.5’’	1°43’16.7’’	3	0	1.6	38	195	-	-	-	-	-	-	-	-
	64	35°03’15.0’’	1°35’19.0’’	10	9	1.2	14	170	191.8	-46.0	191.8	-46.0	199.7	-58.6	2.5	415
ZONE 5 Optimal untilting 0%	54	35°05’43.1’’	1°52’34.8’’	7	4	2.3	12	105	189.6	-57.1	189.6	-57.1	208.0	-56.3	4.5	423
	55	35°01’50.1’’	1°50’06.8’’	8	8	3.15	10	320	190.2	-55.3	190.2	-55.3	181.1	-48.3	7.5	55
	56	35°01’52.4’’	1°51’47.2’’	5	0	4.36	10	320	-	-	-	-	-	-	-	-
	57	35°02’15.5’’	1°51’56.5’’	7	0	4.17	10	350	-	-	-	-	-	-	-	-
	58	35°00’05.7’’	1°49’20.2’’	7	5	6.46	10	330	358.1	12.6	358.1	12.6	357.5	3.7	7.5	105
ZONE 6 Optimal untilting 25%	65	35°04’55.0’’	2°06’42.4’’	10	11	0.8	13	55	179.9	-54.7	183.4	-52.8	191.8	-46.1	3.0	300
	66	35°00’45.4’’	2°05’12.4’’	6	3	3.42	14	105	17.87	46.6	21.6	46.3	31.9	44.1	3.1	1552
	67	35°04’12.8’’	1°59’49.3’’	6	3	11.18	15	270	203.6	-45.2	200	-46.6	187.8	-49.3	6.0	417
	68	34°58’54.0’	2°06’25.1’’	9	6	0.78	30	340	11.3	58.0	6.2	51.4	358.6	30.5	4.3	239
	69	34°57’32.0’’	2°05’26.7’’	9	9	4.43	20	290	15.8	55.5	8.7	54.8	350.4	49.5	1.3	1469
	70	34°58’03.5’’	2°05’56.6’’	10	8	4.11	25	315	14.0	53.6	7.4	50.1	354.5	36.9	1.0	2902
	71	34°59’01.4’’	2°04’52.2’’	11	10	2.5	17	280	217.6	-61.3	210.2	-63.0	184.2	-64.7	2.6	340
	72	34°58’07.1’’	2°05’22.9’’	9	9	1.12	25	315	26.4	46.5	20.5	44.2	7.2	34.4	3.7	198
	73	35°04’12.8’’	1°59’49.3’’	6	4	3.43	15	270	165.9	-49.0	161.8	-48.0	151.2	-43.5	5.6	271
	74	35°04’19.6’’	2°02’07.8’’	6	6	0.57	15	90	185.4	-55.7	190.8	-55.2	205.3	-51.6	5.9	130
	75	35°04’19.6’’	2°02’07.8’’	6	4	0.39	17	90	181.1	-46.8	185.6	-46.6	198.3	-43.8	5.4	286

Table 1

Zone	N sites	D_g(°)	I_g(°)	k	α_{95}(°)	D_{opt}(°)	I_{opt}(°)	k	α_{95}(°)	A_{95}(°)	A_{95Min}(°)	A_{95Max}(°)	D_s(°)	I_s(°)	k	α_{95}(°)
1	12	354.3	44.8	32	7.8	355.5	45.0	32	7.7	7.1	4.4	17.1	6.1	45.2	15	11.7
2	24	16.8	51.7	31	5.4	16.2	50.9	32	5.3	6.3	3.4	11.1	16.2	50.9	32	5.3
3	8	7.2	51.8	52	7.8	8.9	50.4	65	6.9	7.7	5.2	22.1	11.5	47.2	34	9.6
4	10	10.1	43.3	43	7.4	10.1	43.3	43	7.4	-		-	10.0	38.8	17	12.1
5	2	9.9	56.2	-	-_	9.9	56.2	-	-	-		-	23.8	57.3	-	-
4+5	12	10.1	45.4	44	6.6	10.1	45.4	44	6.6	5.9	4.4	17.1	10.4	41.3	18	10.5
6	11	12.3	52.8	63	5.8	10.3	51.4	71	5.4	6.2	4.6	18.1	5.3	46.1	29	8.6
1-6	67	9.3	49.8	33	3.1	9.3	49.1	35	3.0	-	-	-	10.8	45.8	22	3.8
Age																
Upper Miocene	28	3.3	46.6	35	4.7	3.6	46.1	39	4.4	-	-	-	7.0	42.2	19	6.4
Pleistocene	29	17.4	52.5	56	3.6	17.3	51.5	69	3.3	-	-	-	18.1	47.8	42	4.2

Table 2

Zones	Coordinates	$\gamma(°)$	$\gamma_c(°)$	Reversal Test
1	Single polarity			
2	Geographic	2.1	15.3	Positive
	17% untilting	1.5	14.7	Positive
	Stratigraphic	1.6	17.7	Positive
3	Geographic	12.5	13.8	Positive
	35% untilting	9.0	13.4	Positive
	Stratigraphic	9.4	19.7	Positive
4 and 5	Geographic	9.4	16.0	Positive
	0% untilting	9.4	16.0	Positive
	Stratigraphic	22.5	20.5	Negative
6	Geographic	5.9	11.8	Positive
	25% untilting	5.0	11.2	Positive
	Stratigraphic	11.3	16.9	Positive
All zones	Geographic	9.8	6.6	Negative
	Optimal untilting	9.9	6.3	Negative
	Stratigraphic	10.8	7.6	Negative
Zones 2 to 6	Geographic	4.4	6.8	Positive
	Optimal untilting	5.2	6.5	Positive
	Stratigraphic	12.0	8.2	Negative

Table 3

Figure 1a

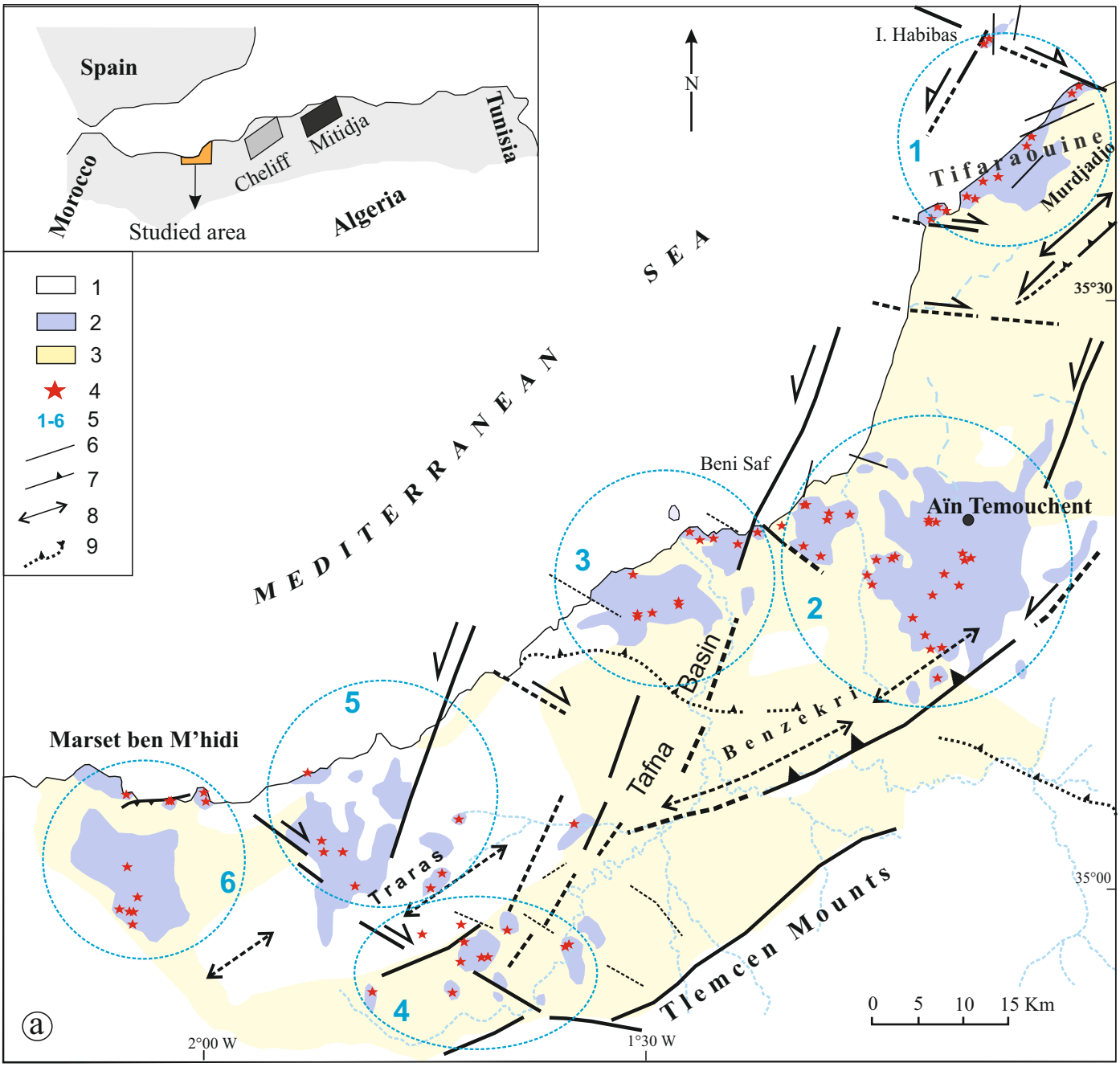
Spain
Morocco
Cheliff
Mitidja
Tunisia
Algeria
Studied area
N
I. Habibas
Tifaraouine
Murdjadjo
35°30
MEDITERRANEAN SEA
Beni Saf
Aïn Temouchent
Basin
Tafna
Benzekri
Marset ben M'hidi
Traras
Tlemcen Mounts
35°00
2°00 W
1°30 W
0 5 10 15 Km
1
2
3
4
5
6
1-6
7
8
9

Figure 1b

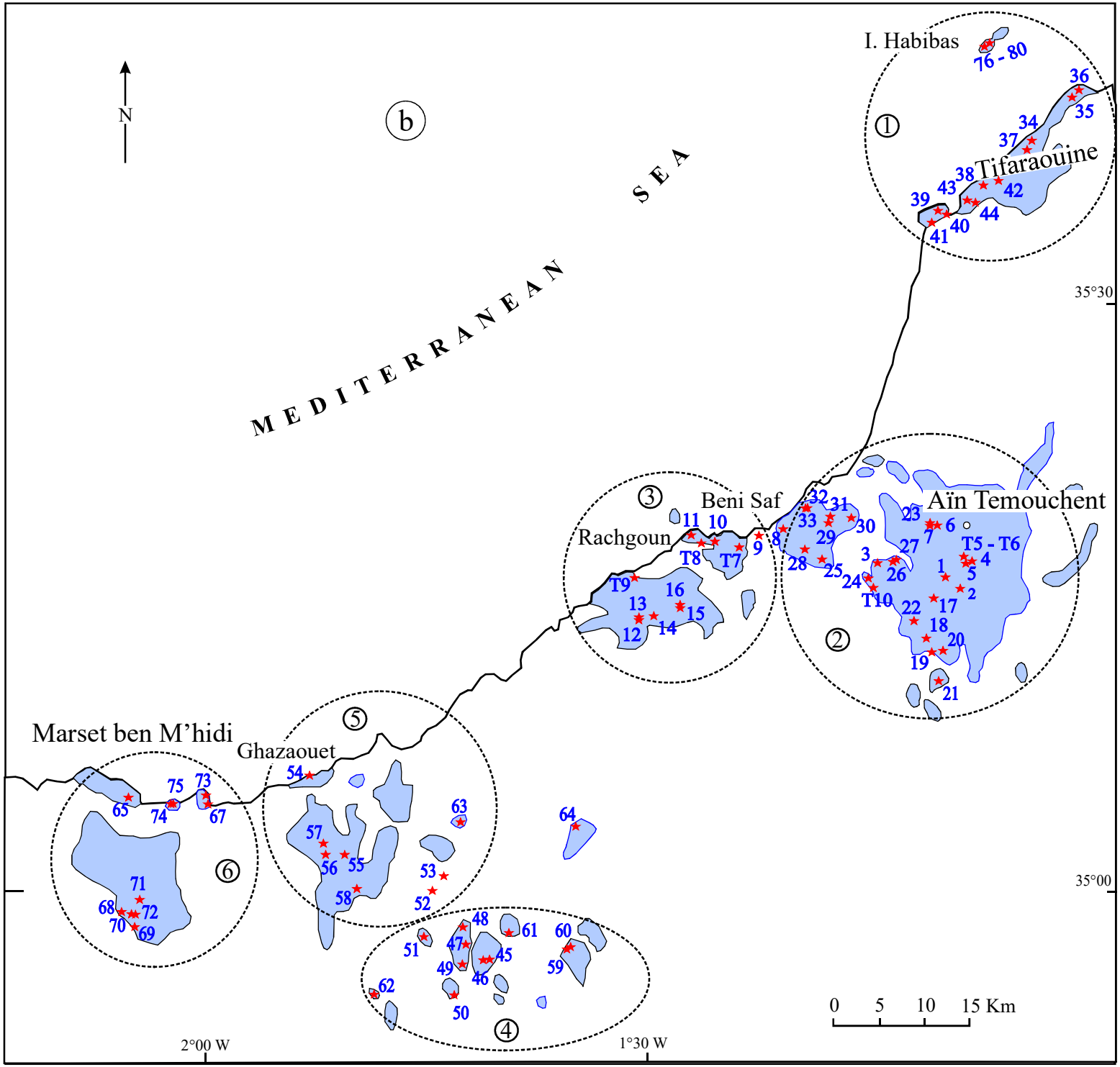
N
b
MEDITERRANEAN SEA
I. Habibas
76 - 80
Tifaraouine
Beni Saf
Rachgoun
Aïn Temouchent
Marset ben M'hidi
Ghazaouet
35°30
35°00
2°00 W
1°30 W
0 5 10 15 Km

Figure 2a

Click here to access/download;Figure;Figure 2a.tif

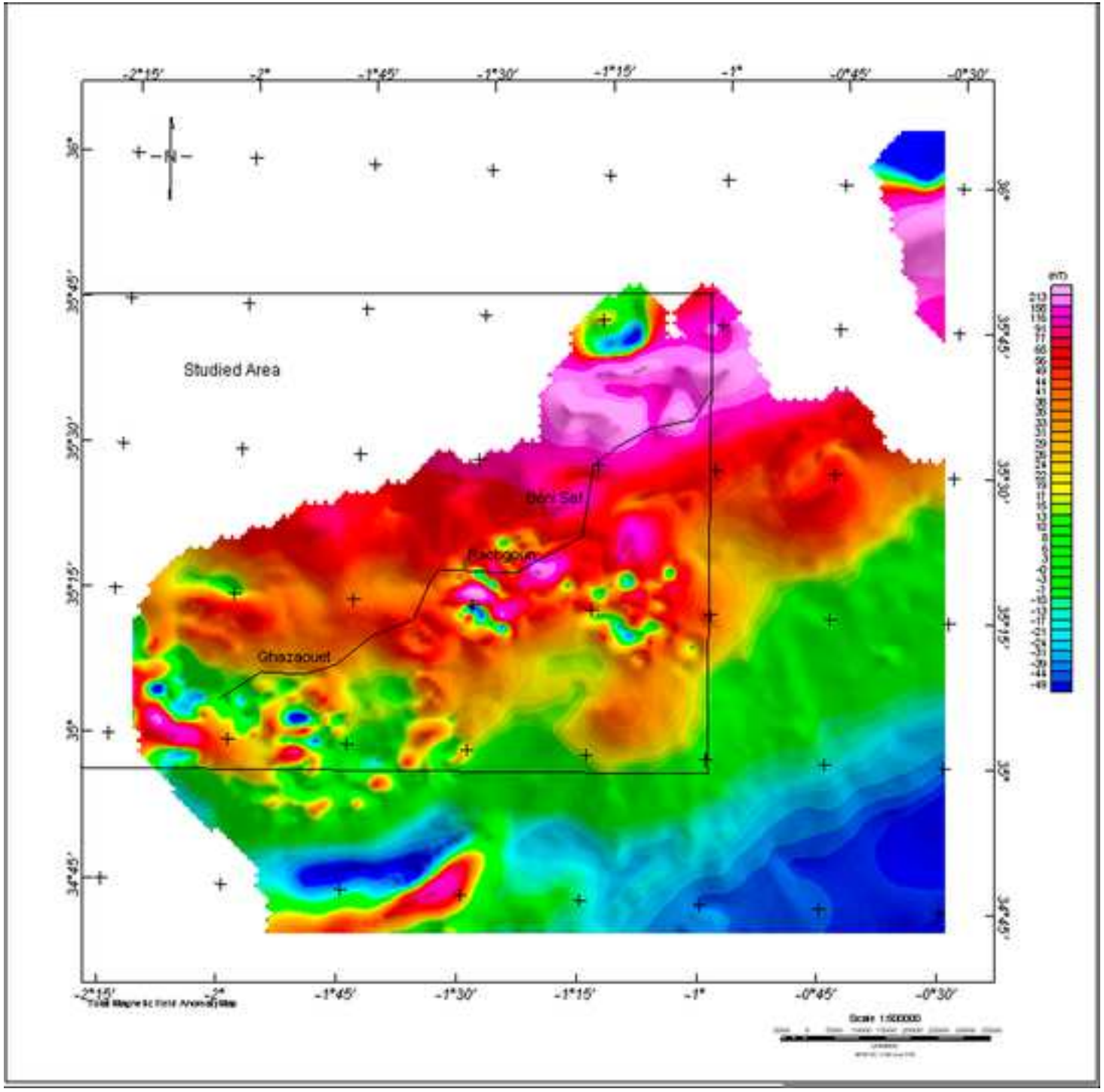

Figure 2b

Click here to access/download;Figure;Figure 2b.jpg

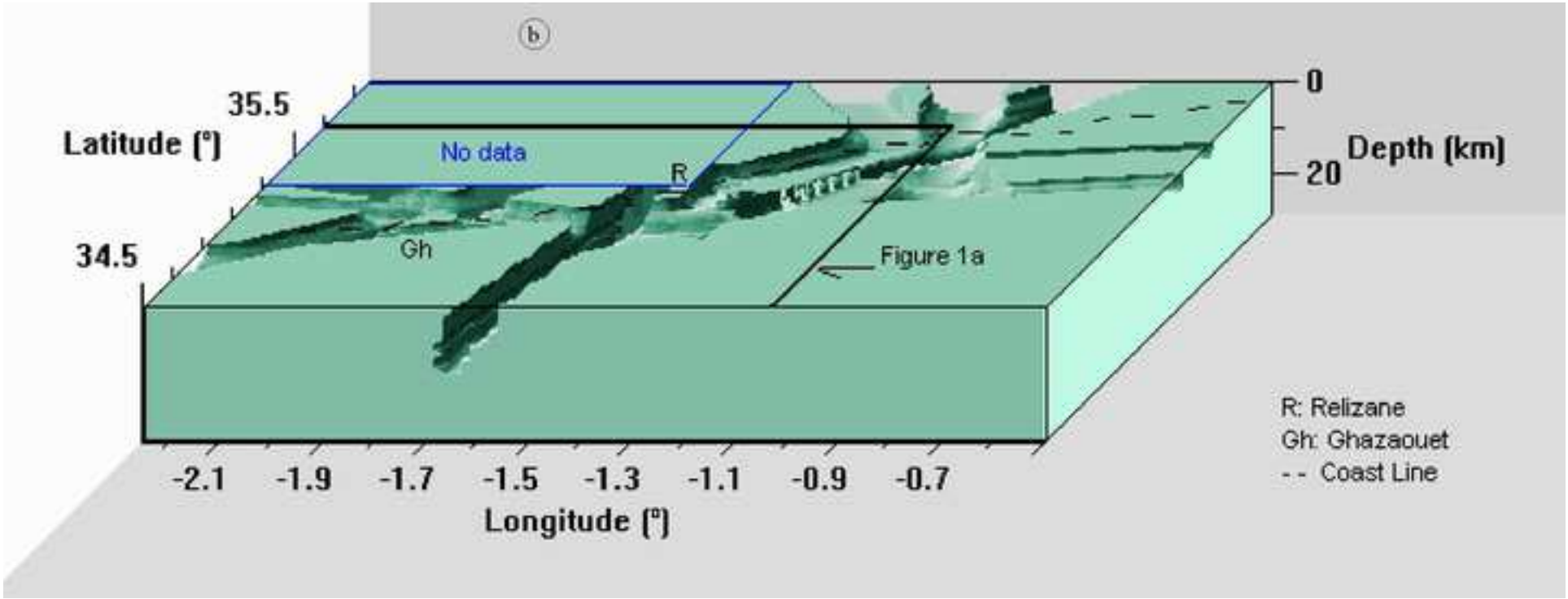

Figure 3

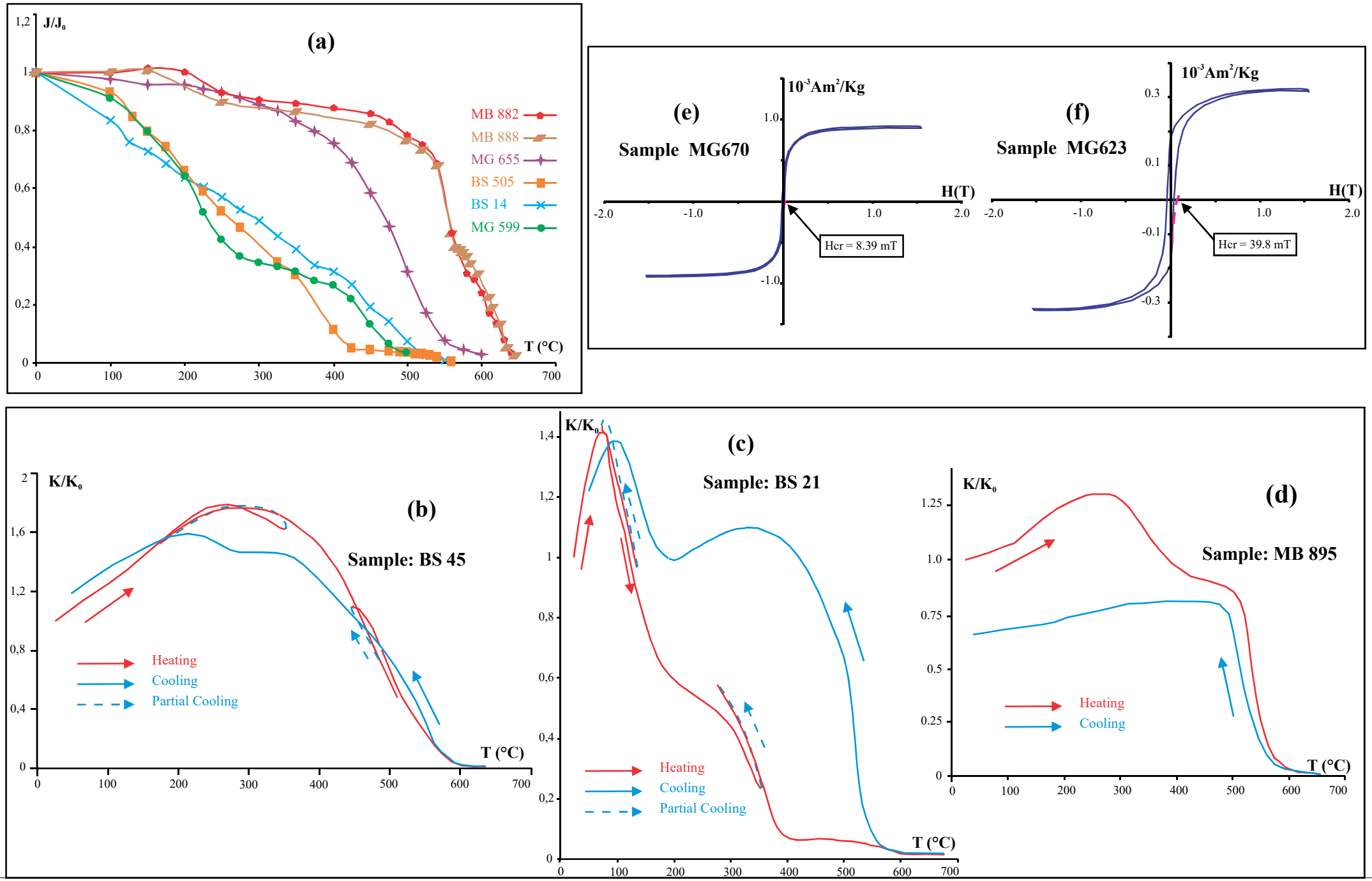
(a)
J/J0
T (°C)
MB 882
MB 888
MG 655
BS 505
BS 14
MG 599
(e)
Sample MG670
10-3Am2/Kg
H(T)
Hcr = 8.39 mT
(f)
Sample MG623
10-3Am2/Kg
H(T)
Hcr = 39.8 mT
(b)
Sample: BS 45
K/K0
Heating
Cooling
Partial Cooling
T (°C)
(c)
Sample: BS 21
K/K0
Heating
Cooling
Partial Cooling
T (°C)
(d)
Sample: MB 895
K/K0
Heating
Cooling
T (°C)

Figure 4

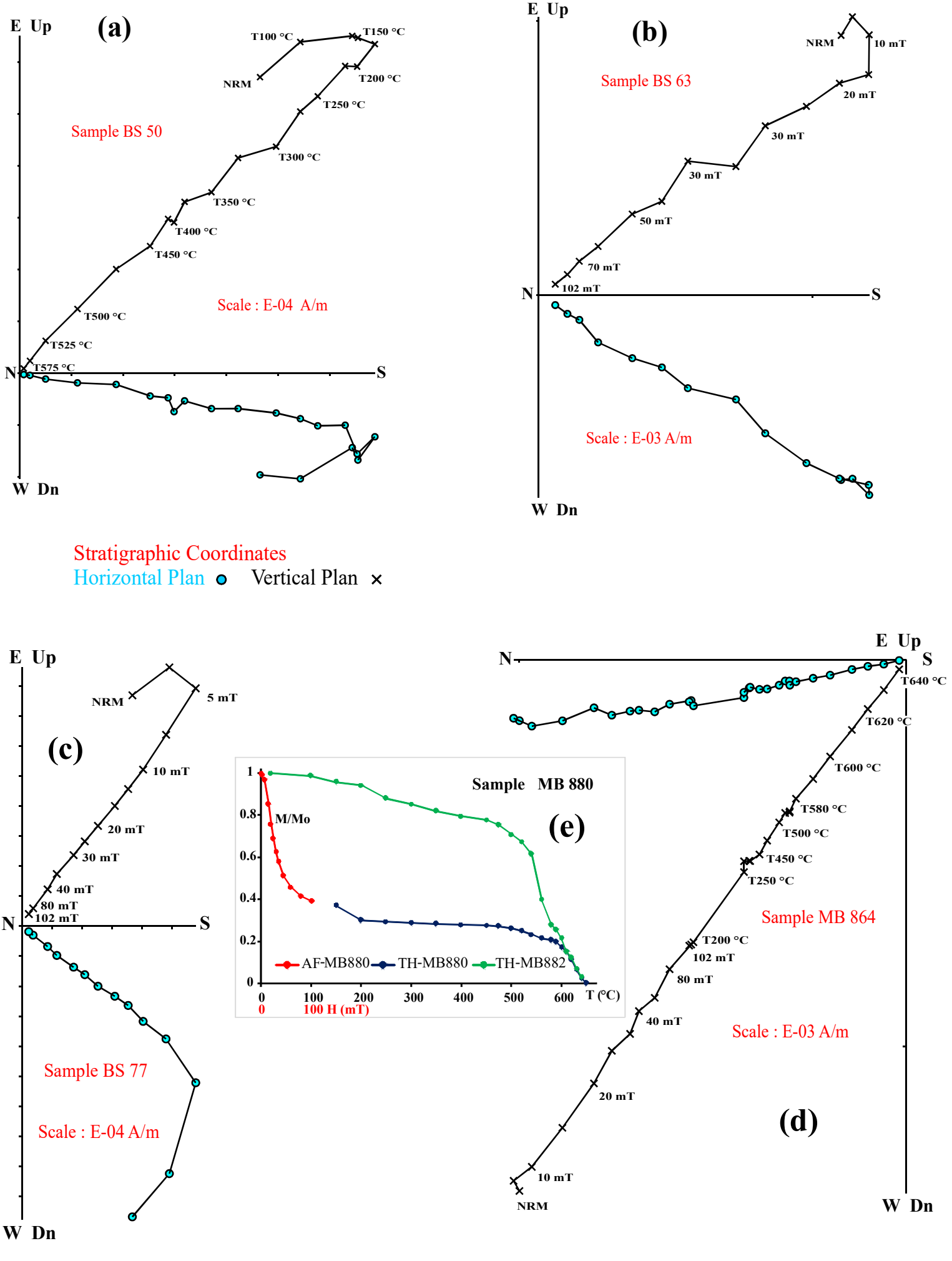
E Up
(a)
T100 °C
T150 °C
NRM
T200 °C
T250 °C
Sample BS 50
T300 °C
T350 °C
T400 °C
T450 °C
Scale : E-04 A/m
T500 °C
T525 °C
T575 °C
N
S
W Dn
E Up
(b)
NRM
10 mT
Sample BS 63
20 mT
30 mT
30 mT
50 mT
70 mT
102 mT
N
S
Scale : E-03 A/m
W Dn
Stratigraphic Coordinates
Horizontal Plan
Vertical Plan
E Up
(c)
NRM
5 mT
10 mT
20 mT
30 mT
40 mT
80 mT
102 mT
N
S
Sample BS 77
Scale : E-04 A/m
W Dn
Sample MB 880
(e)
M/Mo
AF-MB880
TH-MB880
TH-MB882
T (°C)
100 H (mT)
E Up
N
S
T640 °C
T620 °C
T600 °C
T580 °C
T500 °C
T450 °C
T250 °C
Sample MB 864
T200 °C
102 mT
80 mT
40 mT
Scale : E-03 A/m
20 mT
(d)
10 mT
NRM
W Dn

Figure 5

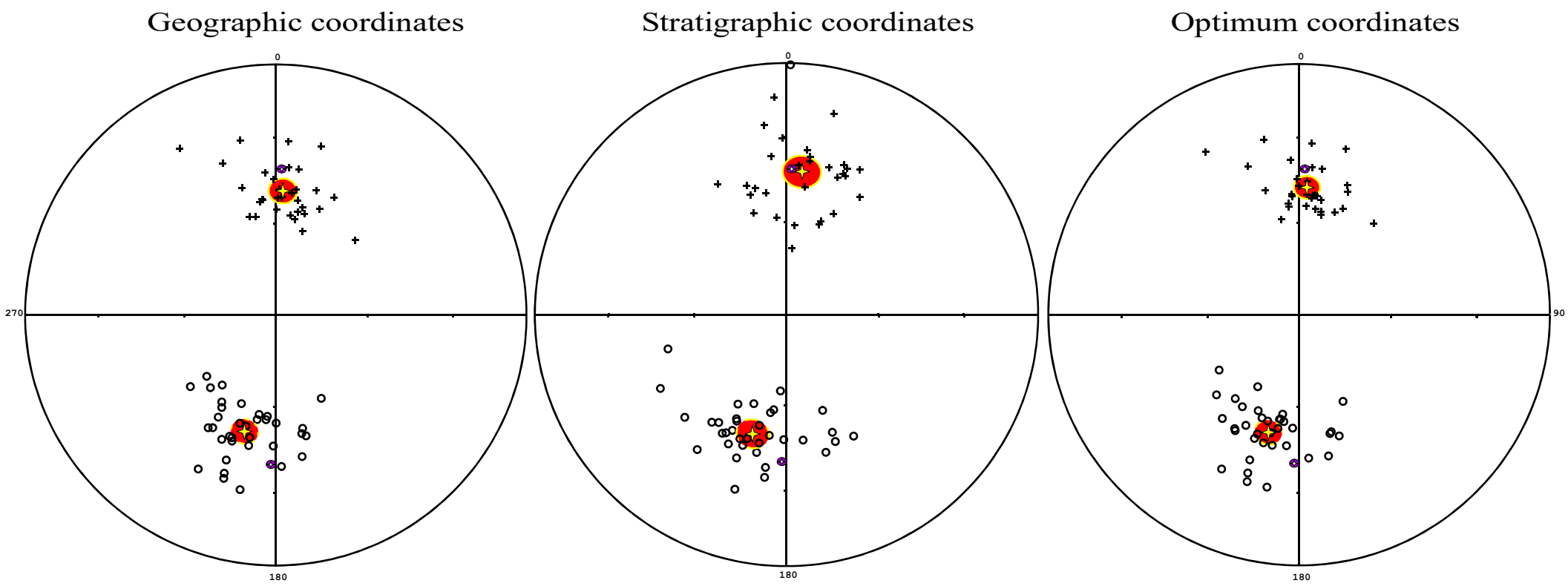
Geographic coordinates
Stratigraphic coordinates
Optimum coordinates
0
90
180
270

Figure 6

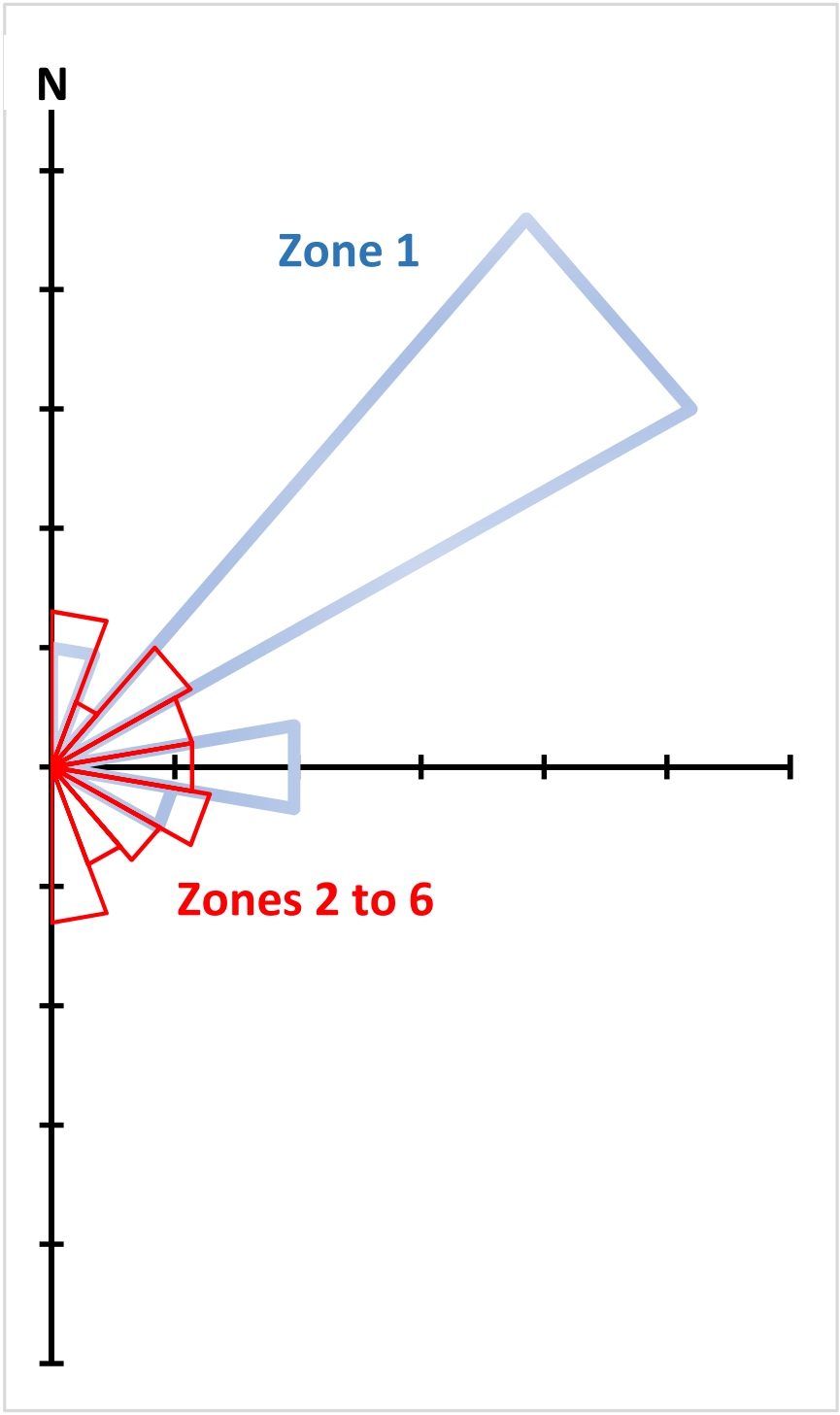

Figure 7

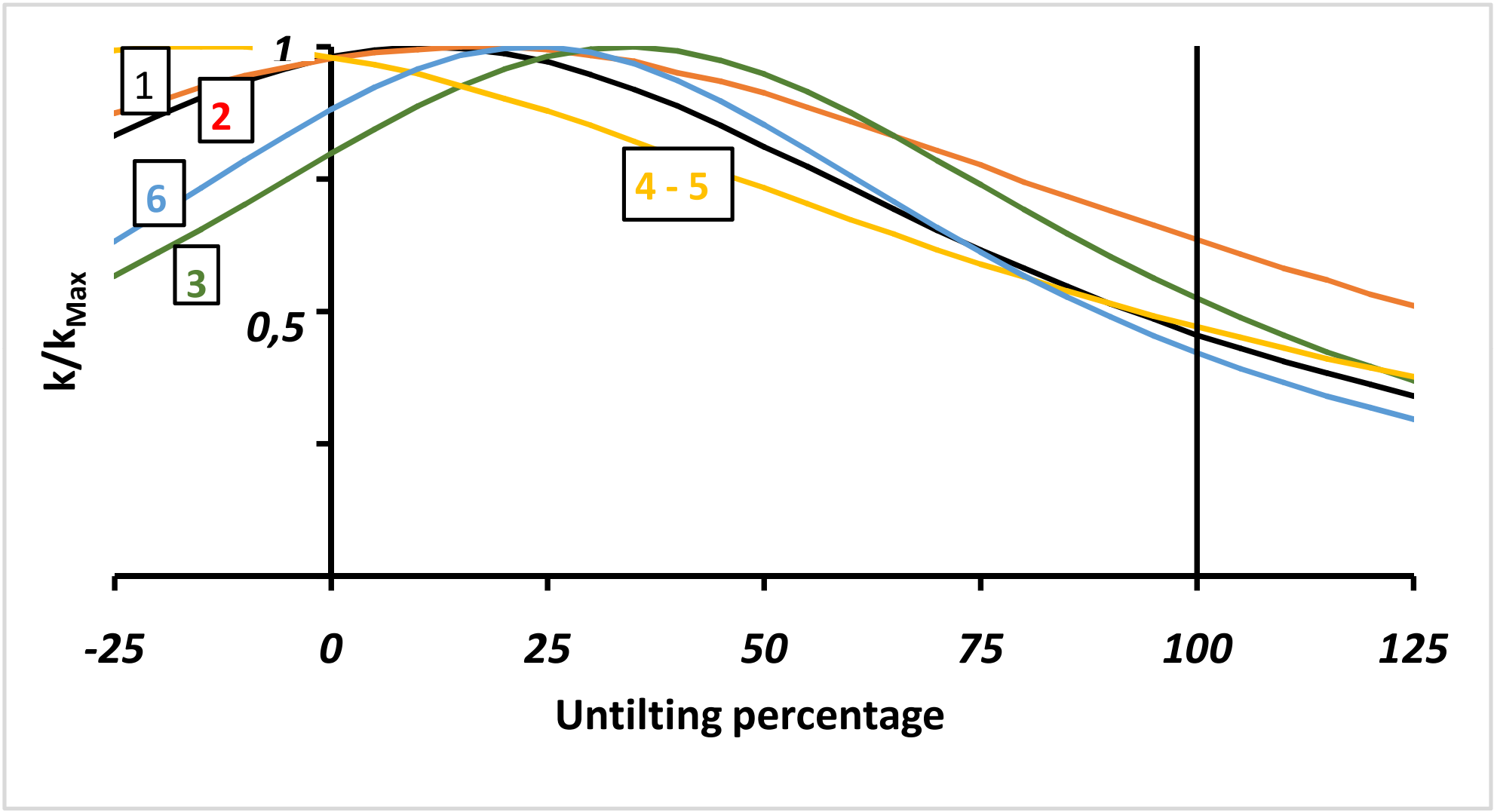

Figure 8

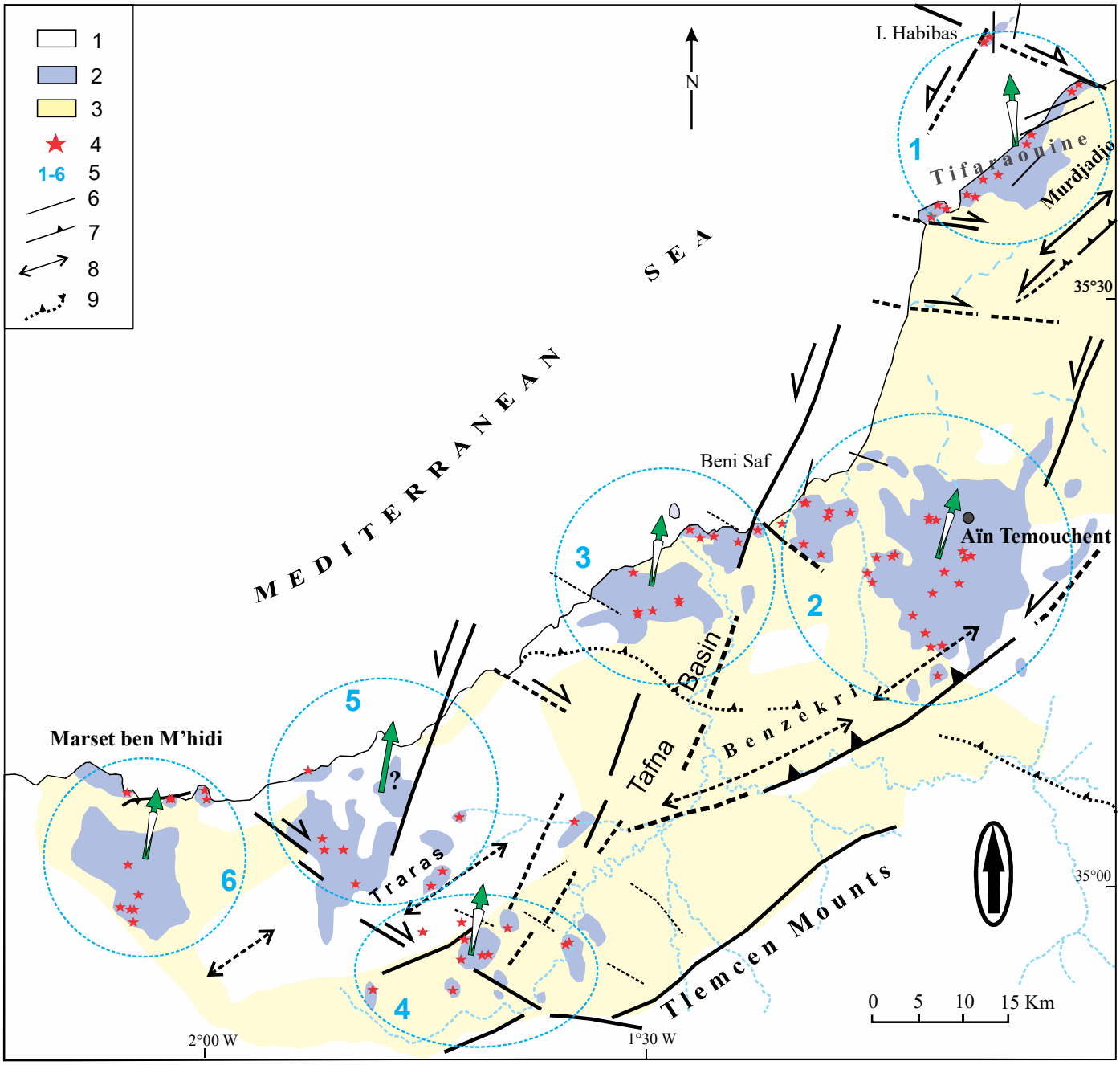
1
2
3
4
1-6 5
6
7
8
9
N
I. Habibas
1
Tifaraouine
Murdjadjo
35°30
SEA
MEDITERRANEAN
Beni Saf
3
2
Aïn Temouchent
Basin
Tafna
Benzekri
5
?
Marset ben M'hidi
6
Traras
4
Tlemcen Mounts
35°00
0 5 10 15 Km
2°00 W
1°30 W

Figure 9

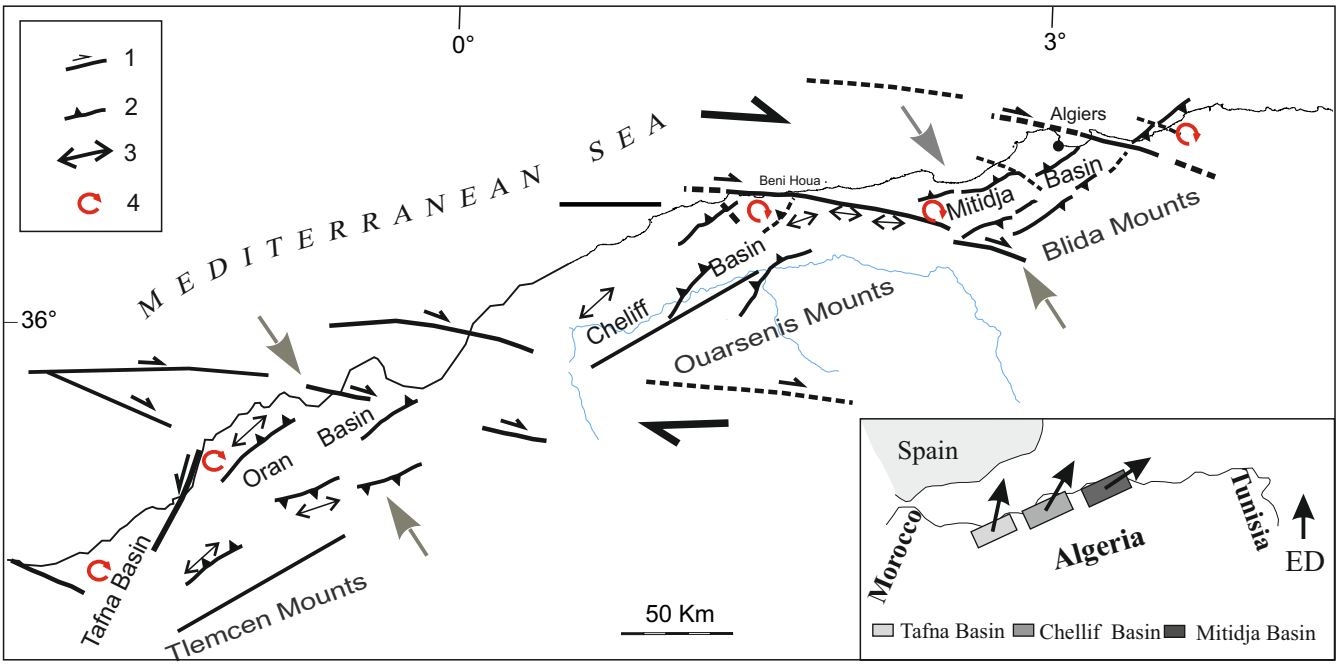
1
2
3
4
0°
3°
36°
MEDITERRANEAN SEA
Algiers
Beni Houa
Mitidja
Basin
Blida Mounts
Cheliff
Basin
Ouarsenis Mounts
Oran
Basin
Tafna Basin
Tlemcen Mounts
50 Km
Spain
Morocco
Algeria
Tunisia
ED
Tafna Basin
Chellif Basin
Mitidja Basin